Magnetic Refrigeration: a Path to Sustainable Hydrogen Liquefaction

Ayush Gupta
Supervisor: Dr. G. R. Blake
Course Coordinator: Dr. P. R. Onck

April 16, 2024

Abstract
The recent interest in hydrogen liquefaction techniques has instigated the exploration of magnetic refrigeration for cryogenic cooling. This has led to the search of materials which exhibit the magnetocaloric effect in the 20-77 K temperature range. The vast majority of compounds that fit the specifications contain critical rare earth elements. Therefore the challenge is to discover sustainable magnetocaloric materials in the cryogenic temperature range. In the context of this challenging task, a handful of prospective compounds have been identified and critically evaluated. Strategies such as doping, which have the potential to tune magnetocaloric properties have been examined. The areas warranting further research in order to realise magnetic refrigeration have been recognized and addressed.

Keywords
Magnetocaloric Effect - Magnetism - Hydrogen Storage - Cryogenic Cooling

Contents

Introduction

Widely regarded as one of the most urgent issues, the increase of global greenhouse gas emissions is contributing to climate change and global warming, profoundly impacting the stability of our society and the environment, and is projected to intensify in the future [1]. In 2023, the global CO_2 emissions from the energy sector reached a record high of 37.4 gigatonnes, increasing the pressure to decarbonize future energy systems [2]. Hydrogen is emerging as a carbon-free energy carrier vital for transitioning to renewable energy sources due to its favourable characteristics, with demand anticipated to undergo rapid growth [3][4][5]. The liquefaction of hydrogen is essential to the storage and transport of the energy carrier, primarily due to the high density at low pressure in its liquid form [4][6]. As the boiling point of molecular hydrogen is 20.3 K, there is an increased interest in developing energy efficient cryogenic refrigeration systems [7][8].

Magnetic refrigeration is a promising solid-state cooling technology, and is based on a refrigerant material that exhibits the magnetocaloric effect [9]. The magnetocaloric effect (MCE) is a magneto-thermodynamic mechanism in which the temperature of the thermally isolated working material can be reversibly changed when an external magnetic field is applied or removed [10]. This effect is brought on by the change in magnetic entropy of the material induced by the order of magnetic moments [11]. The refrigeration cycle consists of two reversible adiabatic (ΔT_{ad}) and isothermal (Δs_{mag}) processes and hence operates as the ideal Carnot cycle (the most efficient cycle working between two heat reservoirs) [3][12][13]. In the specific application of hydrogen liquefaction, the proposed refrigeration cycle operates between a cold reservoir consisting of liquid hydrogen and liquid nitrogen as the hot thermal reservoir [7]. Thus the temperature range of the magnetocaloric working material must be between 20.3 and 77 K in order to be effectively utilized to liquefy hydrogen.

Historically, the vast majority of refrigeration applications have been based on vapor compression technology [9]. As an alternative, magnetic refrigeration offers many benefits over traditional cooling strategies, which make the emerging technology increasingly relevant. As a result of the Carnot cycle, using magnetic refrigeration for cryogenics doubles the efficiency compared to vapor compression [14]. The refrigerants often used in vapor compression systems are ozone-depleting and toxic, magnetocaloric materials avoid this issue and are thus often more environmentally friendly [15]. Furthermore, the application of a solid refrigerant in magnetic refrigeration as opposed to compressors in traditional devices leads to lower

noise levels and a more compact, cost-effective design [3][8]. Besides magnetic refrigeration, magnetocaloric materials also have potential applications in medicine as target drug delivery systems and in cancer treatment (magnetic hyperthermia therapy) [16][17]. In addition, synthesizing magnetocaloric materials into nanoparticles or thin films may yield novel properties that enhance their suitability for applications such as hydrogen liquefaction [12][18].

There are still multiple challenges to overcome in order to realize commercial magnetic refrigeration devices that exploit the magnetocaloric effect. Firstly, suitable magnetic field sources are very expensive and applying a large magnetic field demands significant energy consumption, thus it is paramount to have a working material with a high figure of merit for relatively small volumes [9][16]. Although an extensive number of different magnetocaloric materials have been investigated, discovering the appropriate working material has been the biggest obstacle in realizing magnetic refrigeration and remains to be an active research field [7][14]. Practical requirements of such a magnetocaloric material include economically feasible fabrication and the ability to perform numerous cycles of operation without wear [9]. Arguably one of the principal objectives is to find materials with low criticality in order to achieve sustainable cooling technologies [7][9]. Criticality entails the environmental implications, vulnerability to supply restrictions and the supply risk of materials, which include various economic and geopolitical factors [19]. Therefore, the ambition is to discover materials free of rare earth minerals that exhibit significant MCE and fulfil the other characteristics necessary for hydrogen liquefaction using magnetic refrigeration [20].

In this report, we first introduce the magnetocaloric effect and magnetic refrigeration, delving into the fundamental concepts. Subsequently, the experimental methods that are commonly employed are examined which probe the MCE in materials. Finally, we discuss the various sustainable materials which exhibit potential as solid refrigerants in a magnetic refrigeration device designed for hydrogen liquefaction, providing an overview of the current status and future prospects.

1. Magnetocaloric Effect

In the early 19th century, several scientists started to become intrigued in the relationship between magnetism and heat, and began to formulate theories and predictions based on the experimentation conducted at that time [21]. It was not until 1881 when the magnetocaloric effect was discovered by the German physicist Warburg in iron [22]. French and Swiss physicists Weiss and Piccard also discovered the phenomenon in 1917 (in nickel) and developed the thermodynamic theory to coin the term 'Magnetocaloric Effect' [23]. In the 1920's, Debye and Giauque were the first to recognize the potential applications of the magnetocaloric effect and proposed methods to utilize the mechanism for cryogenic cooling [24][25]. Currently, investigations are underway to demonstrate magnetic refrigeration prototypes as a proof of concept for hydrogen liquefaction [26][27].

The magnetocaloric effect (MCE) is a phenomena which describes the temperature change of a magnetic material under the influence of an external magnetic field. When an external field is applied, the alignment of magnetic moments causes an adiabatic increase in temperature. Conversely, removing the magnetic field results in a temperature decrease.

The MCE is based on the second law of thermodynamics whereby a change in entropy is the reversible heat transferred to the system divided by the temperature [13]. The isothermal heat transfer (ΔQ) between a thermal reservoir and a magnetocaloric material at a temperature T is given by the change in its entropy (ΔS) [28]:

$$\Delta Q = T \cdot \Delta S \tag{1}$$

Where heat is released by the material as its entropy is decreased and a reduction in order will result in the material absorbing heat from its surroundings.

Gadolinium and other rare-earth-based alloys are a widely used point of reference concerning MCE materials [7] [9] [29]. However, such rare earth minerals are scarce and critical, therefore they are not viable for practical applications [30].

1.1 Refrigeration Cycle

The refrigeration cycle for hydrogen liquefaction using magnetocaloric materials is analogous to that of a Carnot engine and is illustrated in the schematic of figure 1 [13]. The magnetic system transfers heat from the cold reservoir to dissipate into a heat bath, therefore the device is thermally insulated from the environment.

The total entropy of a magnetic material is dependent on both the applied magnetic field (H) and temperature (T), and at constant pressure is the sum of the magnetic (S_{mag}), lattice (S_{lat}) and electronic (S_{elec}) components [31],

$$S(T,H) = S_{mag}(T,H) + S_{lat}(T) + S_{elec}(T) \tag{2}$$

The electronic entropy contribution originates from the free electrons in the material and the lattice entropy component is brought about by vibrations in the crystal lattice (known as phonons). Both the electronic and lattice entropy are assumed to be independent of the magnetic H field.

It is evident that the performance of a magnetocaloric material is correlated to the coupling of the magnetic sublattice to an external H field and the resulting magnetic entropy change under magnetization.

The contribution of the lattice and electronic entropy changes to the magnetocaloric effect observed in materials is outside the scope of this review. Theoretically, the lattice entropy can be treated with the Debye approximation, and the electronic entropy can be modelled using the free-electron gas approximation [32].

After absorbing heat from the cold reservoir, an external magnetic field is applied around the magnetocaloric material.

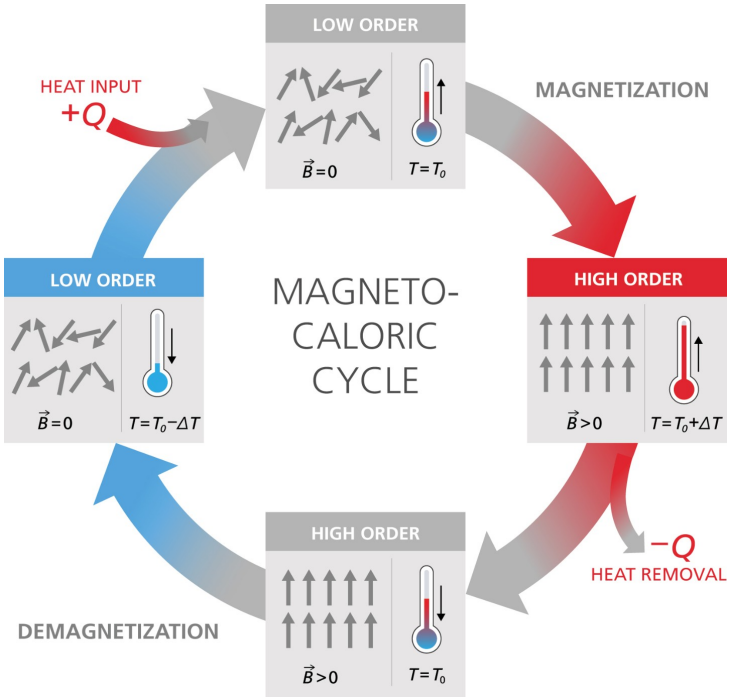

Figure 1. ***Magnetocaloric Refrigeration.*** *First, contacting the magnetocaloric device with the cold reservoir leads to heat input. Applying a magnetic field further increases the temperature before a heat bath absorbs the heat. As the external field is removed, the material cools and the cycle may repeat once more. Figure adapted from [33].*

As a response, the magnetic dipole moments respond by aligning with the field to produce an overall non-zero magnetization. Consequently, the increased magnetic order leads to the reduction of magnetic entropy. As the total entropy of the thermally insulated material must be maintained, the lattice entropy of the material increases as a response, and phonons of higher energy are populated. The result is an adiabatic temperature increase ($T_0 + \Delta T_{ad}$) of the magnetocaloric material.

While the external field remains to be applied (to maintain magnetic order), the gained heat is dissipated as the device is placed in contact with a hot reservoir. The isothermal entropy transfer (ΔS_{mag}) to the reservoir results in the magnetocaloric material returning to its initial temperature, T and is disconnected from the hot reservoir.

Subsequently, the external magnetic field is removed while the device is in thermal insulation. In an ideal scenario, the magnetic dipoles return to their previous random orientation (zero magnetization), destroying the magnetic order. The magnetic entropy increases as the dipoles absorb the heat energy from the lattice (reducing the lattice entropy), thus adiabatically lowering the temperature of the magnetocaloric material to $T_0 - \Delta T_{ad}$.

Finally, while maintaining the external field, the device is placed in thermal contact with the cold reservoir (hydrogen) and thus the refrigeration cycle is completed.

1.2 Thermodynamic Theory

The first law of thermodynamics states that the change in internal energy (dU) is the sum of the heat supplied to the system (dQ) and work done on the system (dW). Assuming that the volume of the system remains constant, the change in internal energy of a magnetic material can be restricted to the heat flux and magnetic work [34],

$$dU = dQ + dW = TdS + \mu_0 H dM \tag{3}$$

Where μ_0 is the magnetic permeability of free space, H is the is the intensity of the applied external magnetic field and M denotes the magnitude of the magnetization of the material.

The change in total entropy of the system can be expressed by the external magnetic H field and temperature T [12]:

$$dS = \left(\frac{\partial S}{\partial T}\right)_{p,H} dT + \left(\frac{\partial S}{\partial H}\right)_{p,H} dH \tag{4}$$

Using the definition of heat capacity and of entropy from the second law of thermodynamics (equation 1), the specific heat at constant pressure and H field can be represented as [13],

$$c_{p,H} = \left(\frac{\partial Q}{\partial T}\right)_{p,H} = T\left(\frac{\partial S}{\partial T}\right)_{p,H} \tag{5}$$

Furthermore, the following Maxwell thermodynamic allows for the entropy dependence on the H field to be expressed as,

$$\left(\frac{\partial S}{\partial H}\right)_{p,T} = \mu_0 \left(\frac{\partial M}{\partial T}\right)_{p,H} \tag{6}$$

Substituting equations 5 and 6 into equation 4 gives:

$$dS = \left(\frac{c_{p,H}}{T}\right) dT + \mu_0 \left(\frac{\partial M}{\partial T}\right)_{p,H} dH \tag{7}$$

An analytic quantification of the MCE can be made when determining the reversible temperature change due to an external magnetic field in an adiabatic process such that $dS = 0$ [35]. By satisfying this condition onto equation 7, one gets the following expression for the reversible adiabatic temperature change (ΔT_{ad}):

$$\Delta T_{ad} = -\mu_0 \int_{H_I}^{H_F} \frac{T}{C_{p,H}} \left(\frac{\partial M}{\partial T}\right)_{p,H} \mathrm{d}H \tag{8}$$

Where H_I and H_F are the initial and final external magnetic fields applied during the adiabatic process.

Another fundamental characteristic quantity of the MCE is the reversible isothermal magnetic entropy change (ΔS_{mag}). In an isothermal process where the H field is changed, equation 7 must fulfill the condition $dT = 0$ giving:

$$\Delta S_{mag} = \mu_0 \int_{H_I}^{H_F} \left(\frac{\partial M}{\partial T}\right)_{p,H} \mathrm{d}H \tag{9}$$

Where again H_I and H_F are the initial and final external magnetic fields applied during the isothermal process.

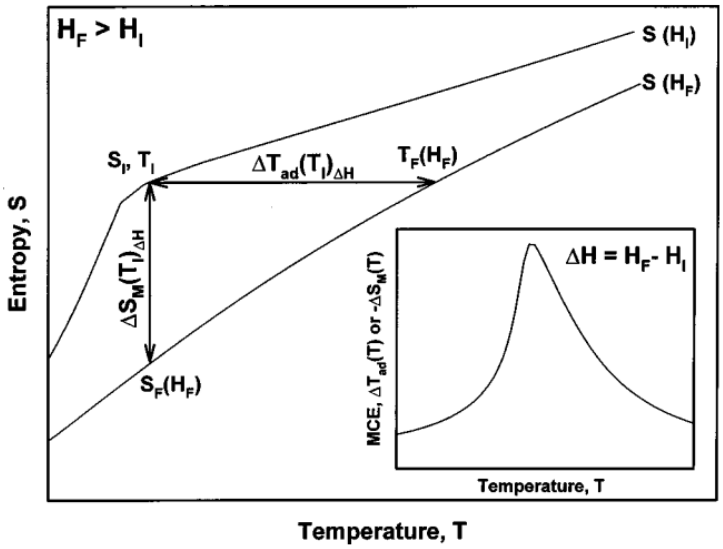

Figure 2. ***Thermodynamic Cycle.*** *A schematic S-T diagram showing the thermal dependency of total entropy of a magnetic material when an external magnetic field is applied ($H_F > H_I$). The reversible adiabatic temperature change ΔT_{ad} and the isothermal entropy change Δs_{mag} due to a change in the external H field are shown. A schematic of the typical MCE magnitude as a function of temperature is shown in the inset, where the peak corresponds to the Curie temperature T_C . Figure adapted from [36].*

The adiabatic process in a magnetic material that leads to ΔT_{ad} is displayed as the horizontal arrow in figure 2. When the magnetic field is increased to H_F, the total entropy of the isolated system remains constant whereas the magnetic entropy decreases. Therefore the temperature rises ($T_F > T_I$) due to an increase in the lattice entropy.

The isothermal entropy change is shown as the vertical arrow in figure 2. As the external H field is increased, the magnetic entropy decreases. As the magnetocaloric material is in thermal isolation, the temperature remains constant and the total entropy of the system also decreases.

From equations 13 and 9 it is important to understand that the sign of $\left(\frac{\partial M}{\partial T}\right)_{p,H}$ determines the type of MCE effect [9]. When the magnetization decreases with increasing temperature, $\Delta T_{ad} > 0$ and $\Delta S_{ad} < 0$ denoting the direct (or normal) magnetocaloric effect (which is plotted in the schematic of figure 2). Meanwhile, a material with an increasing magnetization with temperature exhibits the inverse MCE as $\Delta T_{ad} < 0$ and $\Delta S_{ad} > 0$. This implies a mirroring (across the y=x axis) of the schematic of figure 2, the final temperature and entropy values are switched with the initial whereas the applied magnetic field is still increased (such that $T_I > T_F$ and $S_F > S_I$ while $H_F > H_I$).

Intrinsic properties of materials that result in a larger MCE can be determined by inspecting equations 13 and 9 [35]. Firstly, it is apparent that a larger MCE response is induced when the a large H field is applied or removed. From equation 13 it is also evident that materials with a low specific heat capacity have a MCE at a broad temperature range. For an effective refrigeration application, this temperature range is significant and is required to be at least the same magnitude as the difference in temperatures of the heat baths.

Another important factor to consider when developing and tuning prospective materials, is the Curie temperature (T_C) at which the magnetic (paramagnetic to ferromagnetic) phase transition occurs. From the expressions obtained that describe the MCE, both ΔT_{ad} and ΔS_{mag} are shown to be proportional to the change in magnetization with temperature. The maximum MCE is therefore found to be at the Curie temperature of the magnetic material (as shown in in the inset of figure 2), since the $\left(\frac{\partial M}{\partial T}\right)_{p,H}$ is optimised at this transition temperature [9][37]. This leads to another requirement for a magnetocaloric refrigerant to be used for hydrogen liquefaction, namely that the T_C of the material is between 20.3 and 77 K.

1.3 Phase Transitions

Magnetocaloric materials are categorized according to the thermodynamic order of the phase transition, undergoing either a first-order (FOMPT) or second-order magnetic phase transition (SOMPT) [7].

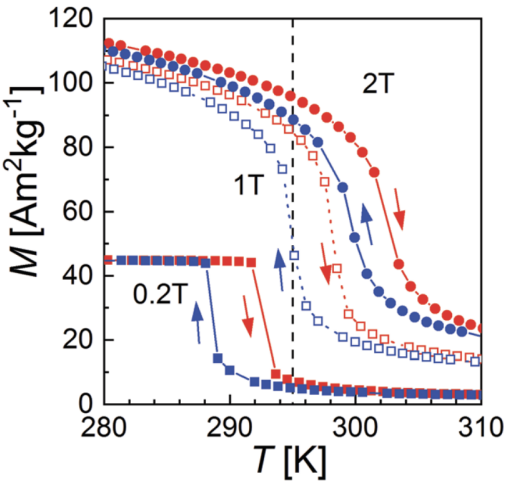

Figure 3. ***First-Order Magnetic Phase Transition.*** *Magnetization measurements as a function of temperature of $La(Fe,Si,Mn)_{13}H_x$ in a magnetic field of 0.2, 1 and 2 T. The vertical dashed line represents the Curie temperature of the material. The discontinuous change of magnetization with temperature is characteristic of a first-order transition. The thermal hysteresis of the magnetization loops is also displayed. Figure adapted from [9].*

Materials with a first-order magnetic phase transition have a discontinuous change in order with respect to temperature, as is shown in figure 3 where the magnetization sharply increases or decreases around the Curie temperature (T_C) [9]. The magnetic transitions in most materials that exhibit FOMPT arises from either a magnetostructural or magnetoelastic transitions [38]. Magnetostructural transitions describe a (reversible) change in crystal structure or lattice symmetry that results in the abrupt transition of magnetization. Whereas magnetoelastic transitions refer to the change in lattice parameters (while ideally preserving crystal structure) that occurs simultaneously with

the magnetic transition.

A characteristic of materials with first-order phase transitions is thermal hysteresis, which is displayed by the magnetization loops in figure 3. This is a major drawback in the context of magnetic refrigeration, causing energy loss during the temperature cycling of the magnetocaloric material as the crystallographic transitions are not completely reversed [9].

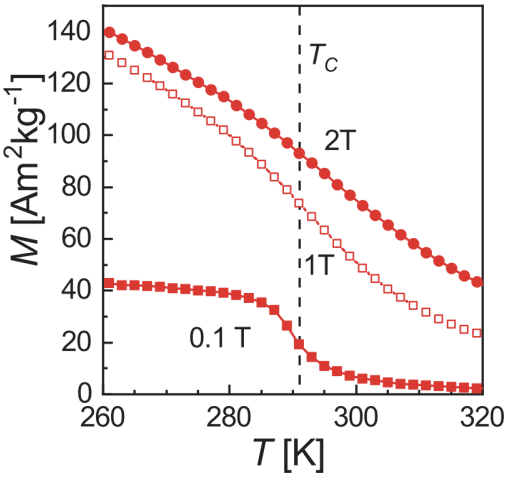

Figure 4. ***Second-Order Magnetic Phase Transition.*** *Magnetization measurements as a function of temperature of gadolinium in a magnetic field of 0.2, 1 and 2 T. The vertical dashed line represents the Curie temperature of the material. The continuous change of magnetization with temperature is characteristic of a second-order transition. Figure adapted from [9].*

When a material undergoes a second-order magnetic phase transition, the magnetic order changes continuously with temperature as is shown by the gradual transition in figure 4. This occurs for example with the benchmark magnetocaloric element gadolinium, with a pure paramagnetic to ferromagnetic phase transition at T_C [9]. Although frequently not exhibiting thermomagnetic hysteresis, SOMPT materials often show a smaller magnitude in the magnetocaloric response [38].

For practical applications, it is favourable for magnetocaloric materials to not exactly have a FOMPT nor a SOMPT, in order to incorporate the distinctive qualities of both [38]. Combining the negligibly thermomagnetic hysteresis characteristic of SOMPT's and the relatively large magnetocaloric effect accompanying FOMPT's.

1.4 Rare Earth Minerals

The majority of materials with a discernible magnetocaloric effect contain rare earth elements, especially for cryogenic refrigeration due to their large magnetic moments and low ordering temperature [7][14]. The lanthanide series of elements contain partially filled $4f$ shells, which is the origin of their large magnetic moment and magnetocrystalline anisotropy [39].

The $4f$ electrons of rare earth elements are highly localised and are very close to the nucleus, and are shielded from the direct environment by the $5s$ and $5p$ orbitals [40]. This results in the probability density of the $4f$ electrons to not overlap with neighbouring atoms, and thus the there is very little direct exchange interaction between rare earth atoms [41]. The magnetic exchange interaction between lanthanides is the indirect Ruderman-Kittel-Kasuya-Yosida (RKKY), where the $4f$ magnetic moments is mediated by delocalised conduction electrons [40]. The exchange interaction has a relatively long range and its nature is dependent on distance. The relatively low exchange integral of rare earth elements results in the low magnetic ordering temperature [42].

The Curie temperature (ferromagnetic ordering temperature) for rare earth elements is proportional to the de Gennes factor (which is different for each lanthanide), and can be written as [41],

$$T_C = \frac{2ZJ}{3k_B} \cdot (g_J - 1)^2 J(J+1) \tag{10}$$

Where the de Gennes factor is $(g_J - 1)^2 J(J+1)$, Z is the nearest neighbours of an atom, J is the exchange constant and k_B is the Boltzmann constant.

2. Figure of Merit

The magnitude of the magnetocaloric effect is described by two fundamental parameters, the reversible isothermal entropy change ΔS_T (often assumed to be equal to ΔS_{mag} as the other change in entropy contributions are negligible) and the adiabatic temperature change ΔT_{ad} [9]. The isothermal entropy change is related to the amount of heat shifted during the refrigeration cycle, as shown by equation 1. While ΔT_{ad} is linked with the temperature span of the magnetocaloric effect.

Reporting the values of the maximum ΔS_T and ΔT_{ad} is not sufficient to effectively determine the magnetocaloric properties of materials, the profile of the curves with respect to temperature is also important. It is desirable for practical applications, that materials exhibit a significant ΔS_T and ΔT_{ad} for a broad operating temperature range, in order to optimise the efficiency of the device [9].

A commonly used figure of merit to effectively asses the magnetocaloric performance of a material is the relative cooling power (RCP). The advantage of this parameter is that it includes the width of the ΔS_{mag} curve to describe the heat exchanged in one cooling cycle [10]. The definition of the relative cooling power is given by [7],

$$RCP = \Delta S_{mag}^{Max} \cdot \Delta T_{FWHM} \tag{11}$$

Where ΔT_{FWHM} is the full-width half maximum (FWHM) of the ΔS_{mag} curve with respect to temperature.

A drawback of the RCP is that the FWHM of the ΔS_{mag} peak often overestimates the operating temperature range of materials with a small MCE (magnetocaloric properties of materials with small but broad ΔS_{mag} curves are exaggerated) [7]. The parameter also neglects the adiabatic temperature change, which is also required to be large for good magnetocaloric materials [9].

Other figures of merit have been formulated to evaluate the magnetocaloric effect, such as temperature averaged entropy change (TEC), coefficient of performance (COP) and reversible heat (Q_{rev}) [7][9]. However these parameters are outside the scope of this review, as they are not commonly reported.

3. Characterisation

In order to simulate and theoretically predict the magnetocaloric properties of materials, various computational models using a mean-field approach is typically used [43]. This allows the estimation of S_T and T_{ad} curves of potential magnetocaloric materials [44].

Machine learning models have been developed and successfully used to explore prospective materials which may show a significant magnetocaloric effect [45]. These make use of statistical analyses from the data in various databases of first-principle calculations [14].

A method to experimentally evaluate the magnitude of the MCE indirectly in materials is to calculate the reversible isothermal entropy change (Δs_T) using magnetic $M-H$ curves [37][46]. By measuring the magnetization M when an external magnetic field is applied H, the field dependent magnetization can be directly determined using superconducting quantum interface device (SQUID) magnetometer setups. The derivation of the isothermal entropy change from thermodynamic theory is shown in section 1.2.

Approximating equation 9 into a summation allows one to calculate the magnetic entropy change as magnetization measurements are conducted with discrete temperature and external magnetic field intervals [37][46].

$$|\Delta S_{mag}| = \sum_i \left[\frac{(M_i - M_{i+1})_{H_i}}{T_{i+1} - T_i} \right] \cdot \Delta H_i \tag{12}$$

Where the consecutive magnetization (M_i and M_{i+1}) and temperature data points (T_i and T_{i+1}) are extracted from a $M-H$ measurement when an external magnetic field (ΔH) is applied with a specific magnitude. In equation 12 it is also apparent that a larger magnetization results in a larger entropy change and thus larger MCE. Furthermore, it is important to note that a larger external field causes a larger magnetization in a typical magnetic material (unless saturation magnetization is achieved). However, this comes at the cost of the energy required to produce the external field. Therefore, even if a material has a large Δs_T, the external magnetic field needed to realise the MCE may be too large for practical considerations.

The reversible adiabatic temperature change (ΔT_{ad}) is also an important direct parameter to evaluate the MCE, there are direct and indirect experimental methods to determine this. A setup involving an adiabatic magneto-calorimeter allows for probing ΔT_{ad} directly under an applied magnetic field [47]. Alternatively, an indirect calculation of ΔT_{ad} can be made when measuring the heat capacity (C_p) at constant external field and using the following approximation [36],

$$[\Delta T_{ad}]_{\Delta H} = -\frac{T}{C_p(T,H)} \cdot \triangle S_{mag} \cdot \triangle H \tag{13}$$

The experimental method to determine the order of the magnetic phase transition that has been widely adopted is the Arrott plot [10]. Using the H field dependence of magnetization measurements, this shows the relationship of M^2 with H/M [48]. The Banerjee criterion states that for first-order magnetic transition materials the Arrott plot has a negative slope, where as a positive gradient is associated to a material with second-order magnetic transitions [49].

4. Prospective Sustainable Materials

In order to design practical magnetic refrigeration devices using MCE and further advance the field, rare earth free magnetocaloric materials have been investigated [50]. However, these specific materials posses a phase transition at room temperature and thus cannot be utilized for hydrogen liquefaction. For a magnetocaloric response in the relevant temperature range (between liquid hydrogen and nitrogen), materials containing rare earth elements are often used [51].

4.1 Spinel Compounds

Spinel compounds are a class of material with a stoichiometry of $A^{2+}B_2^{3+}O_4^{2-}$ where A and B are metals [52]. Specifically, the transition metal oxides that belong to this material category exhibit various interesting interactions between spin, orbital and lattice degrees of freedom, leading to magnetic and ferroelectric phenomena [53]. As depicted in figure 5, the A^{2+} cations lie in the tetrahedral coordination with oxygen cations, and fill an eight of the void volume. Meanwhile the B cations fill a half of the octahedral hole formed of oxygen cations. As a result, the anions of normal spinels form a close-packed sublattice [52].

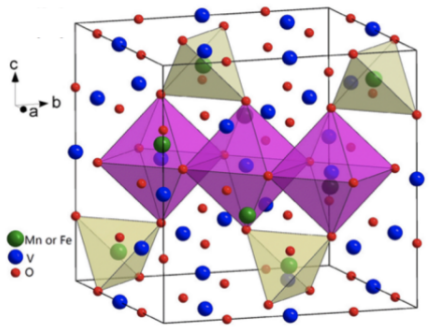

Figure 5. ***Spinel Crystal Structure.*** *Schematic of the crystal structure of $Mn_{1-x}Fe_xV_2O_4$. The tetrahedrally coordinated A sites are shown in yellow whereas the octahedrally coordinated B sites are shown in purple. Figure adapted from [54].*

One of the most promising magnetocaloric materials is the spinel vanadium oxide (MnV_2O_4), as it is a material free of rare earth minerals that exhibits the MCE at temperatures between 20.3 and 77 K [54]. The ferrimagnetic ordering of MnV_2O_4 is relatively complex and several different theoretical models are used to understand the mechanisms [53]. The ferrimagnetism is composed of two antiparallel ferromagnetic sublattices, a short-range direct interaction exists between V^{3+} cations that competes with long-range superexchange interactions between the Mn^{2+} spins mediated by the oxygen 2p orbital.

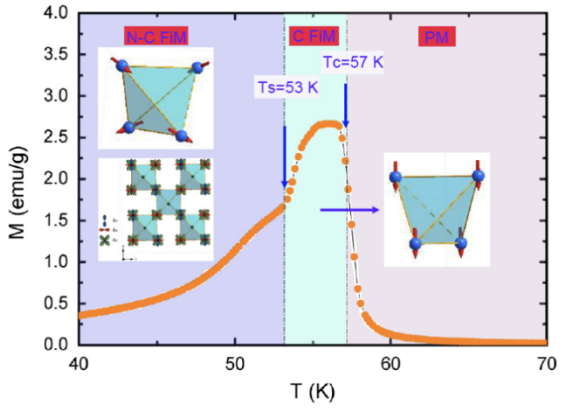

Figure 6. ***Temperature Dependence of Magnetization.*** *Magnetization of MnV_2O_4 as a function of temperature while a magnetic field of 0.002 T was applied in zero-field cooled (ZFC) mode. The non-collinear ferrimagnetic (N–C FiM), collinear ferromagnetic (C FiM) and paramagnetic phases PM are shown along with the temperatures corresponding to the structural phase transition (T_S) and ferrimagnetic ordering (T_C). Figure adapted from [54].*

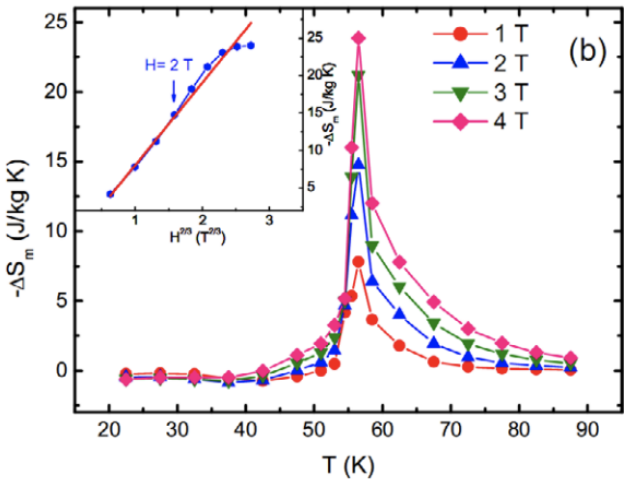

Figure 7. ***Magnetic Entropy Change*** *MnV_2O_4. Entropy changes as a function of temperature extracted from magnetization measurements. H field was switched between 0 to 1, 2, 3 and 4 T. The inset shows ΔS_{mag} versus $H^{2/3}$, follows the linear fit for low fields before deviating. Figure adapted from [54].*

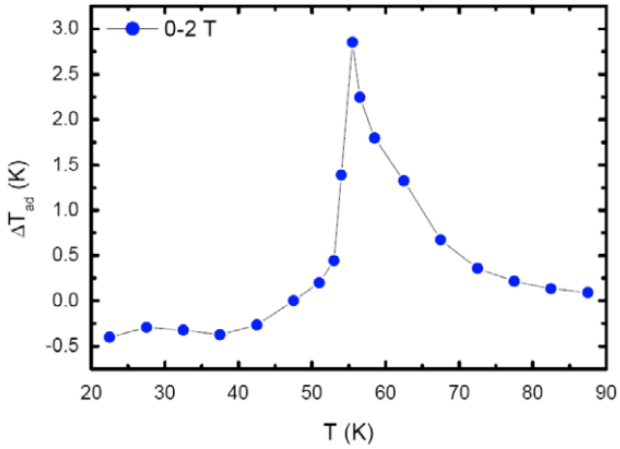

Figure 8. ***Adiabatic Temperature Change*** *MnV_2O_4. Thermal dependence on the temperature change (ΔT_{ad}) of the spinel in a magnetic H field switch of 0-2 T. (ΔT_{ad}) was calculated from ΔS_{mag} data using the specific heat capacity. The peak is visible between $T_S = 53$ K and $T_C = 57$ K. Figure adapted from [54]*

As depicted in figure 6, the material undergoes two different two phase transitions. A paramagnetic-ferrimagnetic transition occurs at a critical temperature of $T_C = 57\ K$ [54]. At a lower temperature, an orbital ordering (OO) transition occurs due to antiferromagnetic interaction between the V^{3+} spins and a Jahn-Teller effect brought on by the VO_6 octahedra [55]. A structural cubic-to-tetragonal structural distortion accompanies the OO transition at a temperature of $T_S = 53\ K$ leading to a canting of the V^{3+} spins and triangular ferrimagnetic ordering such that the systems shows spin frustration and the magnetization decreases [56]. This first-order phase transition shows the strong coupling between the orbital, spin and lattice degrees of freedom. In spite of this, the maximum isothermal entropy change (shown by the peak in figure 7) occurs approximately at T_C, indicating that it is coming from the ferrimagnetic to paramagnetic transition.

The magnetic entropy change curves were calculated from $M - H$ data using equation 9. Figure 7 shows that MnV_2O_4 exhibits a MCE response even at relatively low magnetic fields of 1 and 2 T, which is promising for magnetic refrigeration. A maximum $|\Delta S_{mag}|$ of 14.8 and 24 $J\,Kg^{-1}\,K^{-1}$ are found at magnetic fields of 2 and 4 T respectively.

According to mean field theory, ΔS_{mag} is proportional to $H^{2/3}$ if a second-order magnetic transition takes place [54]. The inset of figure 7 shows a linear relationship that verifies the second-order nature of the magnetic transition. Furthermore, Arrott plots of MnV_2O_4 show a positive slope around T_C which confirms the second-order phase transition [53]. However, for H fields above 2 T the linear relationship no longer holds, this is caused by the first-order structural transition at T_S.

The adiabatic temperature change was calculated using equation 13 with the ΔS_{mag} values and the heat capacity (C_p) of the material. The maximum T_{ad} was found to be 2.9 K. Figure 8 shows an asymmetrical peak of T_{ad} that is centered around T_C. The MCE peaks in figures 7 and 8 are both relatively sharp even for high fields, which is unwanted for magnetic refrigeration applications. The significant MCE effect at temperatures above 54 K show that MnV_2O_4 holds great potential for hydrogen liquefaction. However the lack of a MCE response at lower temperatures (in the region of 20 to 55 K) limits the applicability.

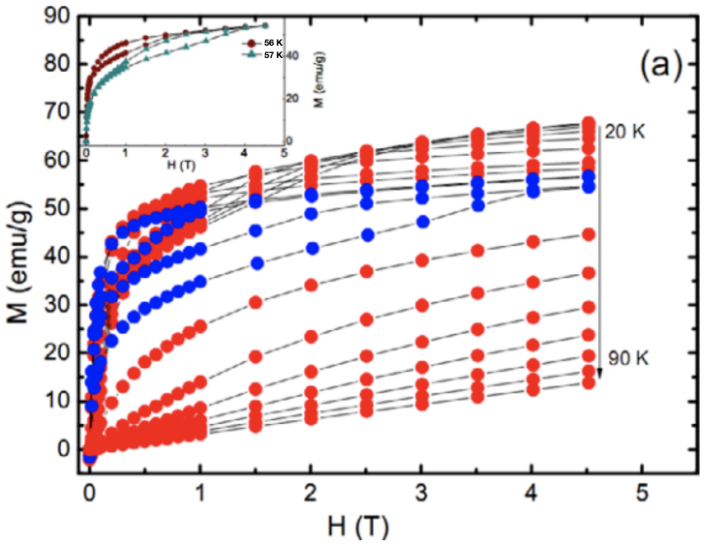

Figure 9. ***Magnetic Hysteresis*** MnV_2O_4. *Magnetization curves across a range of temperatures in a H field up to 4.5 T. The blue markers and the inset show the magnetization curves around the* $T_C = 57$ *K. The hysteresis of the magnetization is apparent for measurements around* T_C. *Figure adapted from [54].*

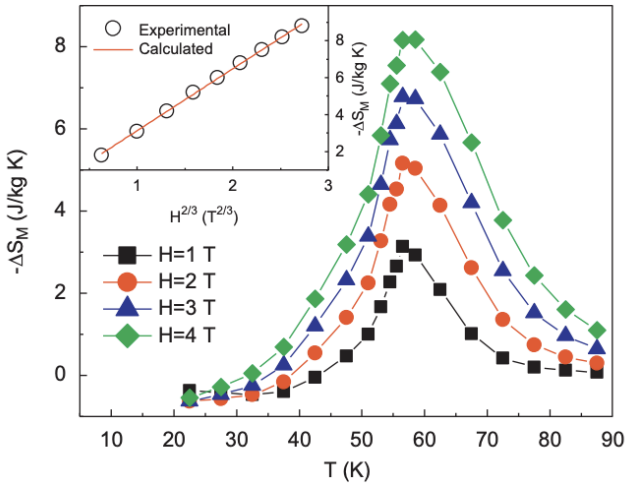

Figure 10. ***Magnetic Entropy Change*** $MnV_{1.95}Al_{0.05}O_4$. *Entropy change as a function of temperature in Al substituted* MnV_2O_4. *Data calculated from magnetization measurements in H fields up to 4 T.The inset shows* ΔS_{mag} *versus* $H^{2/3}$ *near* T_C, *which follows the linear fit. Figure adapted from [56].*

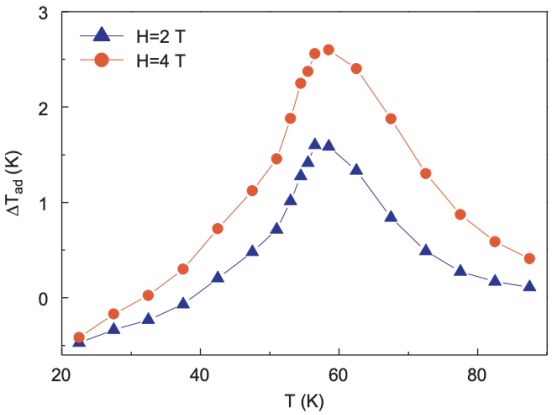

Figure 11. ***Adiabatic Temperature Change*** $MnV_{1.95}Al_{0.05}O_4$. *Relationship between adiabatic temperature change* ΔT_{ad} *and temperature in* MnV_2O_4 *with aluminium B cation substitution. Data was calculated from magnetization measurements and specific heat capacity. Figure adapted from [56].*

Although the MCE in MnV_2O_4 can be attributed to the second-order magnetic phase transition, a significant hysteresis of the magnetization is found around T_C in figure 9. This large hysteresis is a result of the first-order structural phase transition depicted in figure 6. The reversible MCE properties of the material is hampered by the hysteresis, as the performance deteriorates with the refrigeration cycles [9]. Therefore, minimizing the hysteresis loop is one of the aims of further research.

The large MCE response in MnV_2O_4 can be partially attributed to the coupling between the various different degrees of freedom, however further theoretical investigations are necessary to fully understand the complex origin of the large ΔS_{mag}. This may help to optimise the MCE effect in the material in order to fulfil the potential for hydrogen liquefaction applications.

Doping is a relatively common technique used to alter the magnetic properties of materials. In light of this, magnetocaloric investigations have taken place of Al^{3+} doped MnV_2O_4 to create $MnV_{1.95}Al_{0.05}O_4$ [56]. The substitution of Al^{3+} ions of V^{3+} weakens the interaction between V^{3+} ions and strengthens the long range ferromagnetic interactions between Mn^{3+} ions. This causes the spinel structure to exhibit ferromagnetism instead of ferrimagnetism. Furthermore, the Al^3+ impurities leads to the disappearance of the long range orbital ordering and an increase of T_C to 59.6 K [55].

The maximum $|\Delta S_{mag}|$ of 5.2 and 8.2 $JKg^{-1}K^{-1}$ occur at H field changes of 2 and 4 T, lower than the values reported for the undoped MnV_2O_4. Yet, the width of the ΔS_{mag} peaks in figure 10 are significantly broader compared to figure 7. This shows that the Al substitution increases the operating temperature range, which is favourable for applications.

Arrot plots of $MnV_{1.95}Al_{0.05}O_4$ show a second-order magnetic transition [55]. Moreover, the inset of figure 10 shows that ΔS_{mag} has a linear dependence on $H^{2/3}$ across the magnetic field span with no deviation. Compared to figure 7, the absence of deviation in the linear fit suggests that no first-order structural transitions take place, this is a result of the absence of the OO transition and shows a significant advantage of the Al^{3+} doping.

The maximum T_{ad} were calculated to be 1.5 and 2.6 K for H fields of 2 and 4 T, which is also lower than the values reported for MnV_2O_4 (only for 2 T H field). Although the peaks have shifted to the right in figures 10 and 11 after Al^{3+} substitution (corresponding to the increased T_C), the MCE is larger in the lower temperature span of 20-55 K. This is due to the increase in full-width half maximum (FWHM) and the symmetric MCE response with temperature. Hence one can argue that the Al doping has enhanced the operating temperature range.

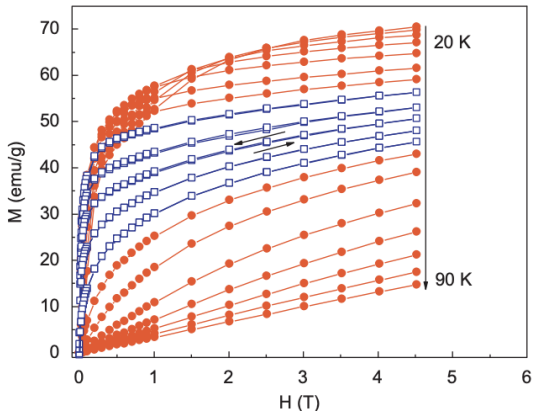

Figure 12. ***Magnetic Hysteresis*** $MnV_{1.95}Al_{0.05}O_4$**.** *Magnetization relative to temperature in an applied H field up to 4.5 T. The blue square markers display the magnetization loops around T_C, which show limited hysteresis. Figure adapted from [56].*

The principal benefit that results from the *Al* doping is the substantial reduction in the magnetic hysteresis. In figure 12 the $M-H$ loops show almost no hysteresis, especially compared to MnV_2O_4 in figure 9. This indirectly shows that there is likely no first-order structural phase transition in $MnV_{1.95}Al_{0.05}O_4$. It is suggested that the coupling between the spin, orbital and lattice degrees of freedom causes the suppression of OO after *Al* substitution [55]. More experimentation on the coupling interactions is necessary to further understand the effects of doping on the magnetic characteristics of spinel structures.

Previous investigations have also included the doping of the transitional metals in spinel crystals. By substituting Fe^{2+} cations in spinel vanadium oxide, $Mn_{1-x}Fe_xV_2O_4$ is produced. Compared to *Mn* orbitals, *Fe* ions do not undergo orbital ordering transitions at low temperatures. Although the specific modifications to the magnetic mechanisms are not yet known, the doping has been shown to affect the lattice parameters and the magnetocaloric response of MnV_2O_4 [57].

For a doping concentration of $x=0.1$, the maximum $|\Delta S_{mag}|$ was found to be 3.8 $JKg^{-1}K^{-1}$, lower than that for MnV_2O_4 and $MnV_{1.95}Al_{0.05}V_2O_4$. The critical temperature was found to be 59, 62 and 67 K (for $x=0.1, 0.2$ and 0.3) whereas the structural transitions caused by orbital ordering were found to occur at temperatures of $T_{OO}=49$, 47 and 43 K [57]. Evidence of thermal hysteresis of the magnetization was also found around the first-order structural phase transitions at T_{OO} [57]. Although, the insets of figure 13 and the Arrott plots show that the material undergoes a second-order magnetic phase transition even at T_{OO}, contradicting the hysteresis data. Therefore, further experimentation is necessary to understand the phase transitions occurring at T_{OO}.

There are several remarkable features of the *Fe* doping that are shown in figure 13. Firstly, it is apparent that the FWHM of the ΔS_{mag} peaks are larger than that of figures 7 and 10. One also observes that the difference between T_C and T_{OO} increases when either the doping concentration or magnetic field strength is increased. This is largely due to a shift of the ΔS_{mag} to higher

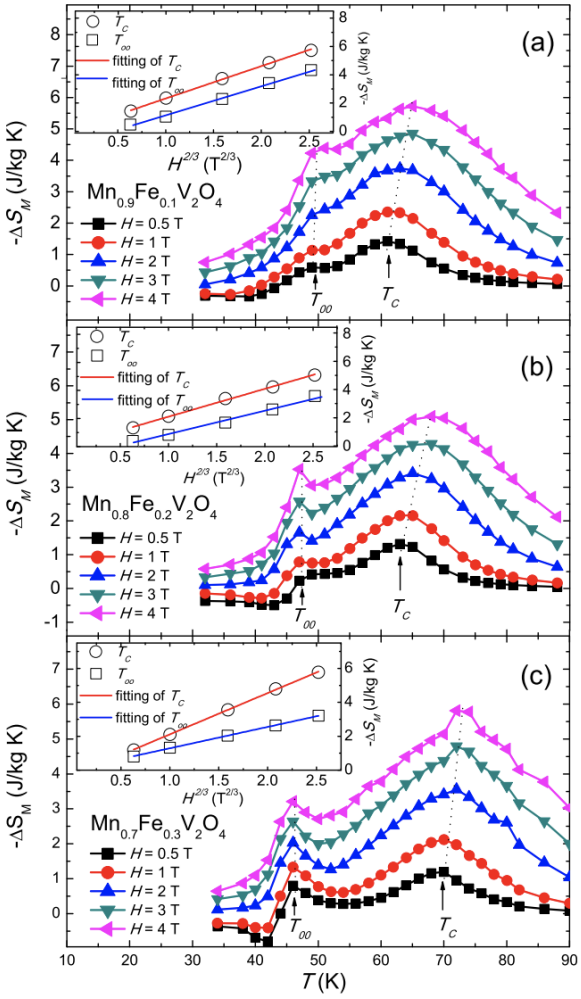

Figure 13. ***Magnetic Entropy Change*** $Mn_{1-x}Fe_xV_2O_4$**.** *Magnetic entropy changes with temperature of MnV_2O_4 with a Fe substitution of $x=0.1$ (a), 0.2 (b) and 0.3 (c). Data extracted from magnetization measurements, separate peaks around T_C and orbital ordering temperatures T_{OO} are visible. The insets show ΔS_{mag} versus $H^{2/3}$ around T_C and T_{OO}, which follow a linear relationship. Figures adapted from [57].*

T_C temperatures when the H field strength is increased. The mechanism behind this has not yet been established. However this result of the doping does increase the operating temperature range of the material which is favourable for applications.

In conclusion, spinel vanadium oxides have shown their magnetocaloric potential despite the lack of rare earth minerals. This is a major advantage towards the sustainable application of magnetic refrigeration in hydrogen liquefaction. Although there are issues with a second-order structural phase transition and resulting thermal hysteresis, they can be mitigated by doping the material. This has also led to larger operating temperature spans (broader ΔS_{mag} and T_{ad} versus temperature peaks). The substitution of vanadium and manganese leads to different intricate magnetic effects, which need to be inspected further. Despite the potential for application, the materials lack a magnetic response for low temperatures relevant for hydrogen liquefaction (between 20 and 45 K). This means that for hydrogen liquefaction, spinel compounds need to be used in

conjunction with other materials (with lower T_C) or manipulated such that a MCE is apparent at lower temperatures (by further experimentation with doping, for example simultaneous *Al* and *Fe* doping or substitution with other non-magnetic elements).

4.2 High Entropy Alloys

High-entropy alloys (HEA) are a relatively new class of materials that represents a novel concept in material design [7]. HEA's comprise of a blend of principal elements in high proportions that form a 'baseless' alloy instead of the traditional alloy design methods that dilute main constituents [58]. These materials focus on the middle portion of elemental phase diagrams to form a high configuration entropy of mixing. Recently, HEA's have received significant attention within material science because of their mechanic and thermodynamic properties [59].

Designing high-entropy alloys in order to maximise their functionality is a major challenge due to wide range of composition possibilities, therefore there are a number of strategies to design these materials [59]. Theoretical predictions of the functional properties in HEA's are also difficult to make [58]. An example of a strategy to maximise the MCE response is to design a material that undergoes a first-order magnetostructural phase transition. Using this technique, the rare earth free HEA $(FeMnNi)_{66.6}(Ge_xSi_{1-x})_{33.3}$ was developed, which undergoes a reversible hexagonal to orthorhombic phase transition [60].

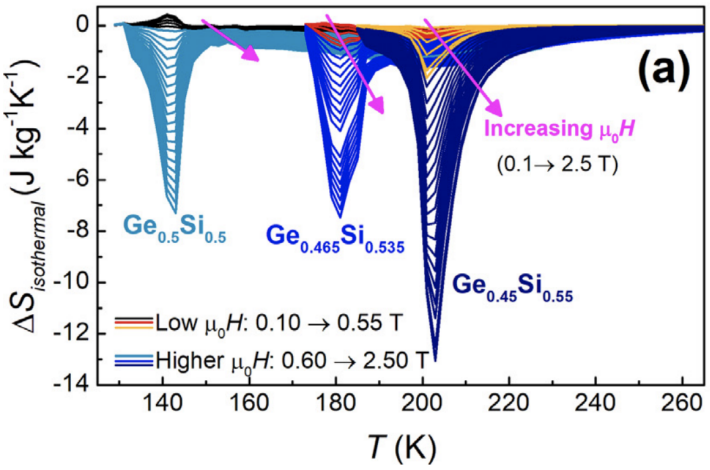

Figure 14. ***Magnetic Entropy Change of HEA*** $(FeMnNi)_{66.6}(Ge_xSi_{1-x})_{33.3}$. *Isothermal entropy curves versus temperature of high-entropy alloys with a composition of* $x = 0.5, 0.465$ *and* 0.435. *Data extracted from magnetization measurements. Figure adapted from [60].*

A ΔS_{mag} of 13.1 $JKg^{-1}K^{-1}$ was found for $(FeMnNi)_{66.6}(Ge_{0.45}Si_{0.55})_{33.3}$ at a temperature of 203 K, the largest value reported for magnetocaloric HEA's [60]. It is also remarkable that this large ΔS_{mag} is achieved with a relatively small H field of 2.5 T. Figure 14 shows that for increasing $Ge : Si$ compositional ratio, the ΔS_{mag} peak decreases in magnitude and temperature. It is argued that the decrease in ΔS_{mag} is due to larger differences between the magnetic ordering Curie temperature T_C and the magnetostructural transition temperature T_M brought on by the change in composition [60].

Characteristic of first-order phase transitions, the HEA studied also exhibits significant thermal hysteresis of its magnetization [60]. Further characterization is necessary in order to establish the consequences of this on the reversible T_{ad} and to asses the severity of the issue. In the context of hydrogen liquefaction, another major issue of this HEA is the high temperature at which the MCE is observed. Although the working temperature can be tuned by changing the composition, it remains to be considerably higher than the boiling point of nitrogen, 77 K.

Another promising HEA is $FeCoCr_xNi$, which has been shown to exhibit the MCE over a wide range of temperatures by altering the stoichiometry and fabrication processes [61]. A component of the fabrication process is cold rolling, in which the thickness of the sample is reduced to the order of $100\mu m$ through a mechanical process. After this step, samples may be heat treated (also called annealing) at high temperature (1073 K) in order to remove defects such as vacancies.

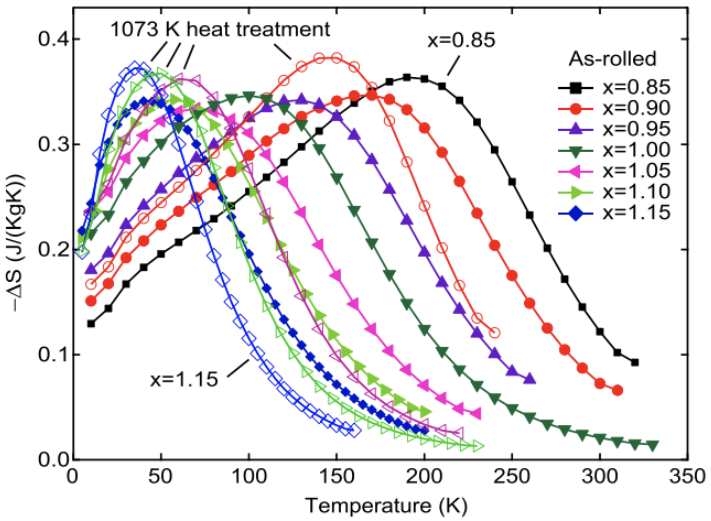

Figure 15. ***Heat Treatment of High-Entropy Alloys.*** *Magnetic entropy change as a function of temperature in a switching magnetic H field of 2 T. High-entropy alloys of various* $FeCoCr_xNi$ *compositions were investigated. The solid markers correspond to samples that were cold-rolled whereas the open markers represent samples that received heat treatment (at* $T = 1073\ K$*) after cold-rolling. Figure adapted from [61].*

Figure 15 shows that although the magnitude of the MCE is relatively small, the FWHM of the ΔS_{mag} peaks are relatively large, and therefore this material has a broad operating temperature range. From the various ΔS_{mag} curves, one may also argue that the heat treatment of samples leads to the narrowing of the peak. Extraction of the temperatures and ΔS_{mag} values of the peaks in figure 15 allows for further analysis

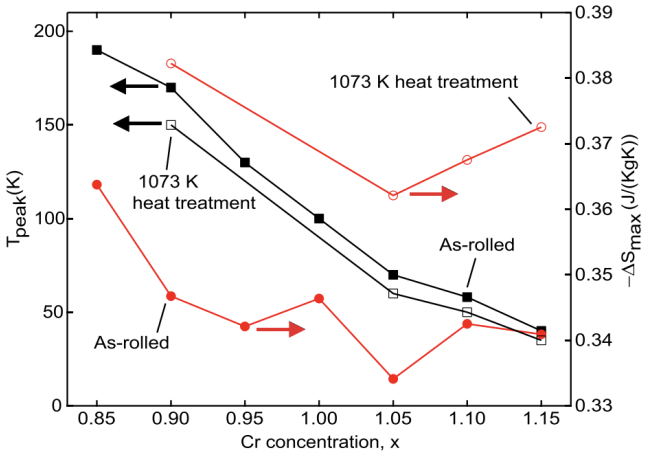

Figure 16. ***Magnetic Entropy Peaks of HEA*** *$FeCoCr_xNi$ Maximum magnetic entropy change (right axis, red markers) and peak temperature (left axis, black markers) of the high-entropy alloy as a function of chromium concentration in a changing H field of 2 T. The solid markers represent samples that were cold-rolled whereas samples that received heat treatment at 1073 K are symbolized by open markers. Figure adapted from [61].*

From figure 16 it is apparent that for both cold rolled and annealed samples, a higher concentration of chromium concentration leads to decreasing peak temperature values. This is because the addition of the non-magnetic metal leads to weaker exchange interactions present in the material, thus reducing the magnetization. Furthermore, the Cr addition also generally leads to a reduction in the magnitude of ΔS_{mag}.

The heat treatment of samples during fabrication leads to an increase of the maximum observed ΔS_{mag}, as is evident from the red markers of figure 16. Annealing at 1073 K also induces a decrease in the temperature at which the peak of the ΔS_{mag} occurs. It is argued that as a result of the local stoichiometric disorder (due to defects) introduced by cold rolling, the magnetic atoms are less likely to have chromium atoms as nearest neighbours, and thus have stronger exchange interactions [61]. Meanwhile, the annealing procedure activates the thermal vacancies leading to long-range chemical order and therefore lower Curie temperatures.

To conclude, HEA's are complex materials where it is difficult to model the mechanisms behind the magnetic properties. $(FeMnNi)_{66.6}(Ge_xSi_{1-x})_{33.3}$ is an example of a HEA with large ΔS_{mag} magnitudes, however the operating temperature range is too high for it to be practical for hydrogen liquefaction. On the other hand, $FeCoCr_xNi$ exhibits the MCE in a wide span of temperatures, yet the magnitude of the ΔS_{mag} is modest. Altering the composition of non-magnetic atoms in HEA's has found to impact the MCE characteristic significantly. Avenues for further research include assessing the affects of altering the composition of magnetic atoms in HEA's. Attempts to model the magnetic interactions in HEA's will allow for the optimization of the magnetocaloric properties.

4.3 Light-Rare Earth Materials

Light-rare earth elements (Lre) consist of the lanthanides with atomic numbers ranging from 57 to 62 (lanthanum, cerium, praseodymium, neodymium, promethium, and samarium) [62]. These minerals have been proposed as possible sustainable alternatives to heavy-rare earth elements, due to their relative abundance in the Earth's crust [63]. Yet, Lre's have also been evaluated as critical metals on account of the environmental challenges faced in mining, hence other more sustainable methods to acquire the Lre are being explored. [62].

Replacing heavy-rare earth minerals with light-rare earth elements in compounds to develop a somewhat sustainable material that exhibits the MCE, is an ongoing field of research. Specifically, light-rare earth Laves phases with a stoichiometry of $LreAl_2$ $(Lre : Nd, Pr, Ce)$ are being investigated for applications in hydrogen liquefaction. The magnetism in these intermetallic compounds arises between the interplay of magnetic exchange interactions (between the rare earth atoms) and the crystalline electric field (CEF) [64]. The CEF can partially remove the degeneracy of the total angular momentum in lanthanides, thereby influencing the number of magnetic states at low temperatures (and the magnetocaloric effect) [65]. The CEF interaction is the result of the charges in the neighbours of the magnetic atoms [32].

Magnetocaloric characteristics have been reported for the Laves phases $PrAl_2$ (with a $T_C = 32.5\ K$) and $NdAl_2$ (with a $T_C = 77\ K$) [66]. The width of the ΔS_{mag} and ΔT_{ad} peaks (with respect to temperature) is not large enough to cover the full temperature span necessary for hydrogen liquefaction. By doping these Laves phases with other Lre's that have different de Gennes factors, the Curie temperature of the materials can be tuned (as shown by equation 10) in order to cover the 20-77 K temperature range [63].

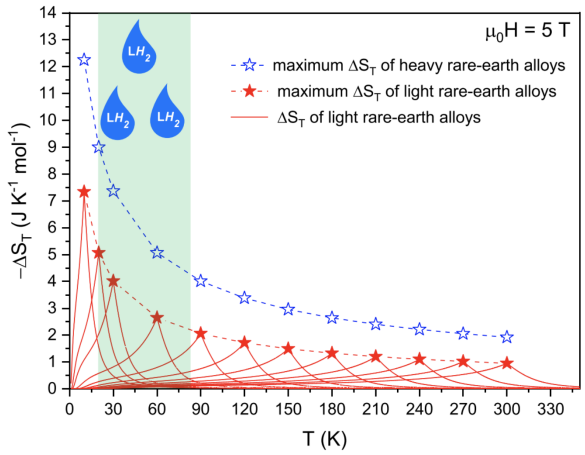

Figure 17. ***Theoretical Isothermal Entropy Change of Ideal Nd- alloy family.*** *Isothermal entropy change as a function of temperature with a switching H field of 5 T, calculated using the mean-field model. The red markers indicate the ideal alloys of the light-rare earth Nd while the blue markers correspond to the ideal alloys of the heavy-rare earth Dy. The green shaded area represents the temperature range relevant for hydrogen liquefaction (20-77 K). Figure adapted from [63].*

Theoretical mean field models were used to compute the isothermal entropy change (ΔS_T, sum of the modelled magnetic and lattice entropy components) of idealised Nd- alloys where the T_C was varied while the other material parameters remained constant [63]. Figure 17 serves as a proof of concept for Lre Laves phases as magnetic refrigerants for hydrogen liquefaction. A significant ΔS_T response is exhibited within the 20-77 K temperature range, where the magnitude of the entropy change increases with lower T_C. Although theoretical ΔS_T curves for ideal Dy- alloys demonstrate a larger MCE, the light-rare earth alloys show potential for application in hydrogen liquefaction.

In practice, ideal alloys where only the T_C parameter changes do not exist, hence doping the Laves phases to create $Nd_{1-x}Pr_xAl_2$ and $Pr_{1-x}Ce_xAl_2$ allow for the tuning of the Curie temperature.

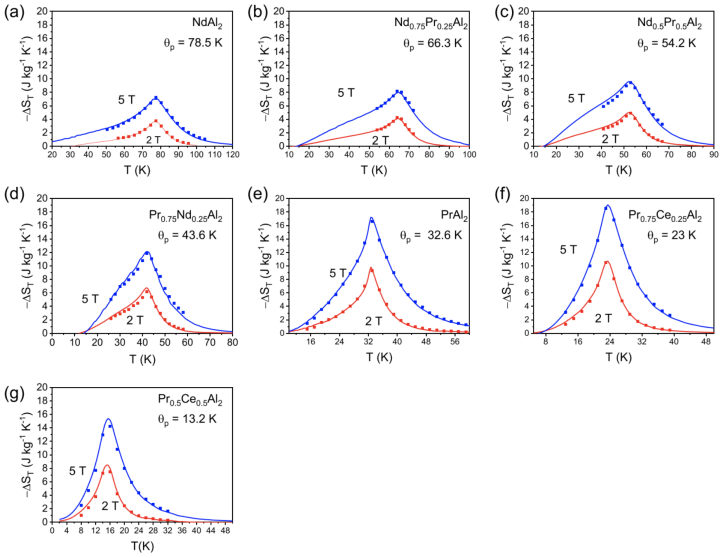

Figure 18. ***Isothermal Entropy Change of*** $LreAl_2$ ***Alloys.*** *Experimentally extracted from magnetization measurements, the alloys of* $Nd_{1-x}Pr_xAl_2$ *where* $x = 0$ *(a), 0.25 (b), 0.5 (c), 0.75 (d), 1 (e) and* $Pr_{1-x}Ce_xAl_2$ *where* $x = 0.25$ *(f), 0.5 (g) were investigated for H fields of 2 and 5 T. The* T_C *of the alloys were tuned such that the relevant operating temperature range was covered. Figures adapted from [63].*

Of the alloys that were investigated at a switching H field of 2 T, $NdAl_2$ exhibited the lowest ΔS_T peak of 3.67 $JKg^{-1}K^{-1}$ whereas $Pr_{0.75}Ce_{0.25}Al_2$ showed the largest MCE with a ΔS_T of 10.48 $JKg^{-1}K^{-1}$. As predicted in figure 17, the magnitude of ΔS_T increases for the alloys with lower Curie temperature. Yet, figure 18 shows that $Pr_{0.5}Ce_{0.5}Al_2$ is en exception to this trend, as the ΔS_T peak is lower than that of $Pr_{0.75}Ce_{0.25}Al_2$. It is hypothesized that the decrease in entropy change is partially caused by the crystal electric field [63]. The ΔS_T peaks in figure 18 are relatively narrow and the FWHM seems to increase slightly with alloys of lower T_C. Nonetheless, the intricate tuning of the T_C by changing the stoichiometry results in alloys with ΔS_T curves that overlap in temperatures with one another, hence allowing for a magnetic refrigeration device to be designed that can be utilized for hydrogen liquefaction.

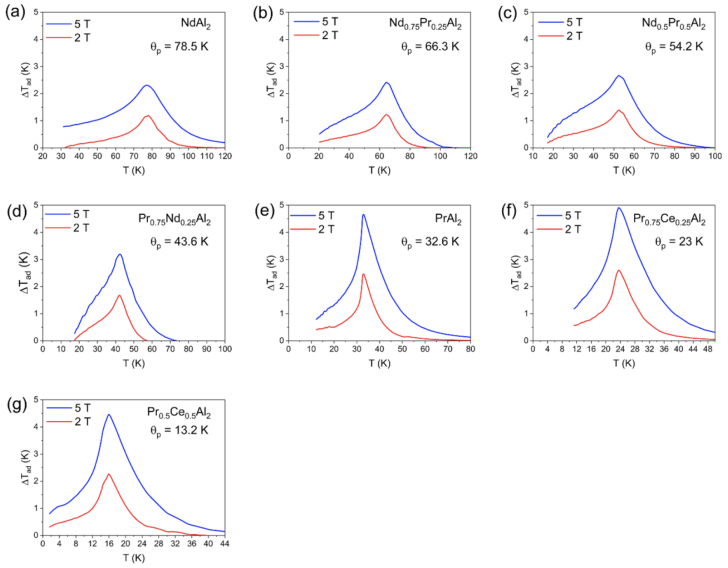

Figure 19. ***Adiabatic Temperature Change of*** $LreAl_2$ ***Alloys.*** *(Experimentally extracted from heat capacity measurements, the alloys of* $Nd_{1-x}Pr_xAl_2$ *where* $x = 0$ *(a), 0.25 (b), 0.5 (c), 0.75 (d), 1 (e) and* $Pr_{1-x}Ce_xAl_2$ *where* $x = 0.25$ *(f), 0.5 (g) were investigated for H fields of 2 and 5 T. The* T_C *of the alloys were tuned such that the relevant operating temperature range was covered. Figures adapted from [63].*

Figure 19 shows that the adiabatic temperature change ranges from 1-2.5 K for the various alloys. A general trend of increasing ΔT_{ad} of alloys with lower T_C is observed, with $Pr_{0.5}Ce_{0.5}Al_2$ being noted as the exception.

Another method to combine the magnetocaloric properties of $PrAl_2$ and $NdAl_2$ to achieve a 20-77 K temperature span is to form a composite of the two Laves phases.

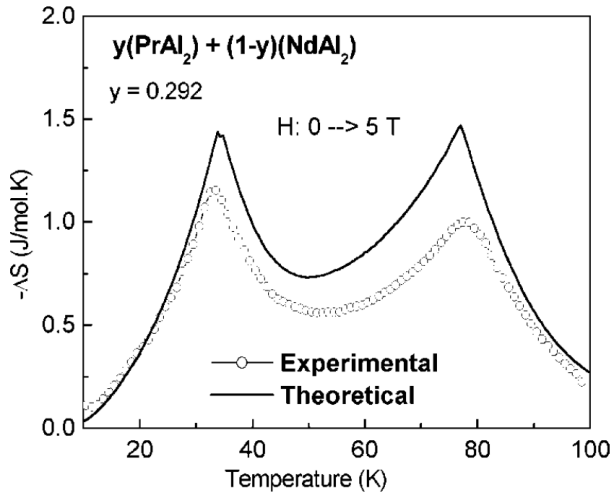

Figure 20. ***Magnetic Entropy Change of Composite*** $0.292(PrAl_2) + 0.708(NdAl_2)$**.** *Magnetic entropy change as a function of temperature for a composite of* $PrAl_2$ *and* $NdAl_2$ *using a switching H field of 5 T. The open circular markers represent the experimental data extracted from magnetization measurement whereas the solid line corresponds to calculations from a theoretical model. Figure adapted from [66].*

This entails forming a hybrid material of the two Laves phases in specific molar proportions to form $y(PrAl_2) + (1-y)(NdAl_2)$. Where the constant y (molar ratio) depends on the switching magnetic H field strength used [64]. The resulting ΔS_{mag} curve often covers a large temperature range, exceeding that of the single Laves phases. Such a table-like ΔS_{mag} profile is desirable for refrigeration devices utilizing the Ericsson cycle (alternative to the Carnot cycle), which ideally employs a material with a constant ΔS_{mag} for the temperature range [67].

The optimum molar ratio for a magnetic switching of 5 T was found to be $y = 0.292$ [66]. Figure 20 shows a ΔS_{mag} with two peaks and a broad characteristic with a temperature range approximately between 25 to 85 K. Comparing with figure 18 shows that the magnitude of ΔS_{mag} of the composite is lower than that of the individual component Laves phases. The applicability of such a ΔS_{mag} profile to an Ericsson or Carnot cycle is beyond the scope of this review. Furthermore, comparisons between the performance of devices using the Carnot and Ericsson cycle are important in order to develop materials for magnetic refrigeration.

Producing samples in a melt-spun ribbon form have been shown to affect the magnetic and thus the magnetocaloric properties of intermetallic materials. Specifically for the $DyNi_2$ Laves phase, the maximum ΔS_{mag} has been shown to increase when preparing the samples in melt-spun ribbons compared to bulk [64]. It is claimed that the increase in magnetocaloric peaks arises from the texture of the melt-spun ribbons, which affects the magnetic properties. Furthermore, it is argued that hysteresis effects (which are unfavourable for applications) are reduced with texture [64].

The favourable magnetocaloric properties of light-rare earth Laves phases motivates the search of other novel materials that may exhibit the MCE. For example, the intermetallic compounds $LreMn_2$ and $Lre2Mg_2$ have not yet been investigated despite the magnetocaloric potential [7]. The strategy to replace heavy-rare earth minerals for light-rare earth alternatives in already established magnetocaloric materials is also an interesting direction for further material research. Although, extensive analysis on the criticality and sustainability of light-rare earth elements needs to be conducted in order for the materials to be viable for applications.

4.4 $ReNi_5$ Compounds

Among the prospective magnetocaloric materials for practical applications is the family of compounds with a stoichiometry of $ReNi_5$ ($Re \equiv$ rare earth element). Although containing rare earth elements, these compounds have a relatively low content of these minerals and also have a relatively low cost [68]. The series of materials crystallizes in the $CaCu_5$-type structure with the hexagonal P6/mmm space group [69]. The magnetic behaviour stem from the exchange interactions of the rare earth atoms and the crystalline electric field (CEF) [70]. Of the series of compounds, a handful are relevant for the operating temperature range in the context of hydrogen liquefaction.

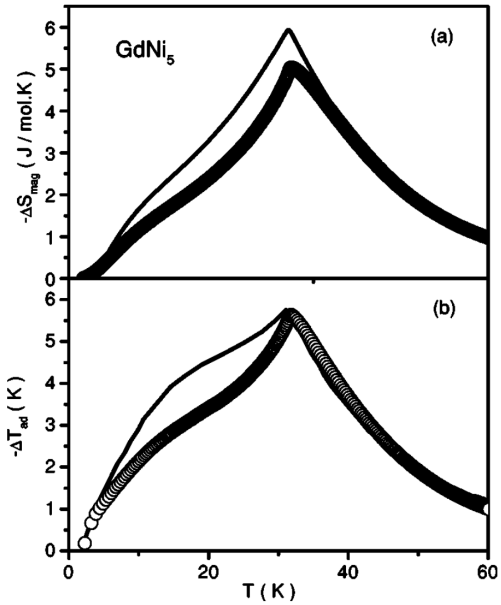

Figure 21. ***Magnetocaloric Effect of*** *$GdNi_5$. Magnetic entropy change (a) and adiabatic temperature change (b) as a function of temperature for $GdNi_5$ using a switching H field of 5 T. The open circular markers represent the experimental data and the solid line corresponds to theoretical calculations. Figure adapted from [70].*

$GdNi_5$ is an example of a material suitable for hydrogen liquefaction due to a Curie temperature of 32 K. From figure 21, the ΔS_{mag} is found to be approximately 2.25 $JKg^{-1}K^{-1}$ and the ΔT_{ad} approximately 5.5 K. The commonly used magnetocaloric gadolinium, results in a broad ΔS_{mag} and T_{ad} peak respective to temperature, which is favourable for applications. A drawback of using $GdNi_5$ for hydrogen liquefaction is the low MCE observed for the high temperature range close to the boiling point of nitrogen (50-70 K). $TbNi_5$ was also shown to have a promising magnetocaloric characteristic for hydrogen liquefaction, with a T_C of 23 K it has similar issues as $GdNi_5$.

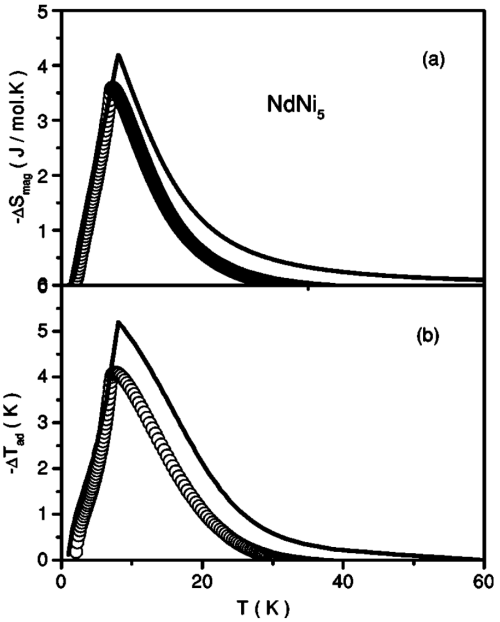

Figure 22. ***Magnetocaloric Effect of*** $NdNi_5$. *Magnetic entropy change (a) and adiabatic temperature change (b) as a function of temperature for* $NdNi_5$ *using a switching H field of 5 T. The open circular markers represent the experimental data and the solid line corresponds to theoretical calculations. Figure adapted from [70].*

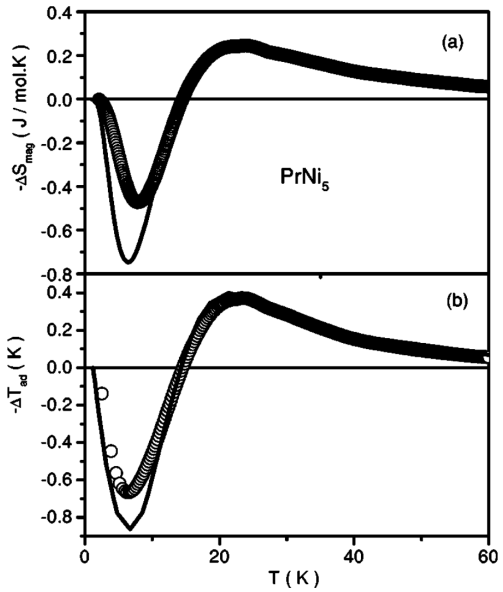

Figure 23. ***Magnetocaloric Effect of*** $PrNi_5$. *Magnetic entropy change (a) and adiabatic temperature change (b) as a function of temperature for* $PrNi_5$ *using a switching H field of 5 T. The open circular markers represent the experimental data and the solid line corresponds to theoretical calculations. Figure adapted from [70].*

Nd_Ni_5 is an interesting material due to the use of the light-rare earth element neodymium (which are more abundant in nature). With a T_C of 8 K, the maximum ΔS_{mag} was found to be approximately 1.58 $JKg^{-1}K^{-1}$ and the T_{ad} to be approximately 4 K. The magnetocaloric peaks in figure 22 show limited MCE response in the 20-60 K temperature region and therefore tuning of the material is required for applications in hydrogen liquefaction.

$PrNi_5$ utilizes the rare earth element praseodymium in order to exhibit magnetocaloric behaviour. Figure 23 shows that below 14 K, the material displays the inverse magnetocaloric effect, where the magnetic entropy increases when the external magnetic field is applied. It is argued that the inverse characteristics originate from CEF effects [70]. At temperatures higher than 14 K, the normal magnetocaloric effect is observed in the compound with a T_C of 21 K. From figure 23, the magnetocaloric response was found to be relatively modest with a S_{mag} of approximately 0.091 $JKg^{-1}K^{-1}$ and a ΔT_{ad} of approximately 0.35 K. For practical applications, the MCE must be arguably enhanced and the temperature range increased to include the span of 35-77 K.

Doping $ReNi_5$ compounds with ferromagnetic elements have been found to drastically change the MCE, specifically the substitution of nickel with cobalt or iron in $TbNi_5$ has been investigated [71]. The doping of these magnetic atoms leads to the exchange interactions between the 3d orbitals of the transition metals and between the rare earth element and the transition metal, thereby increasing the Curie temperature.

The substitution of nickel with magnetic elements significantly increases the T_C of the alloy. The doping of iron raises

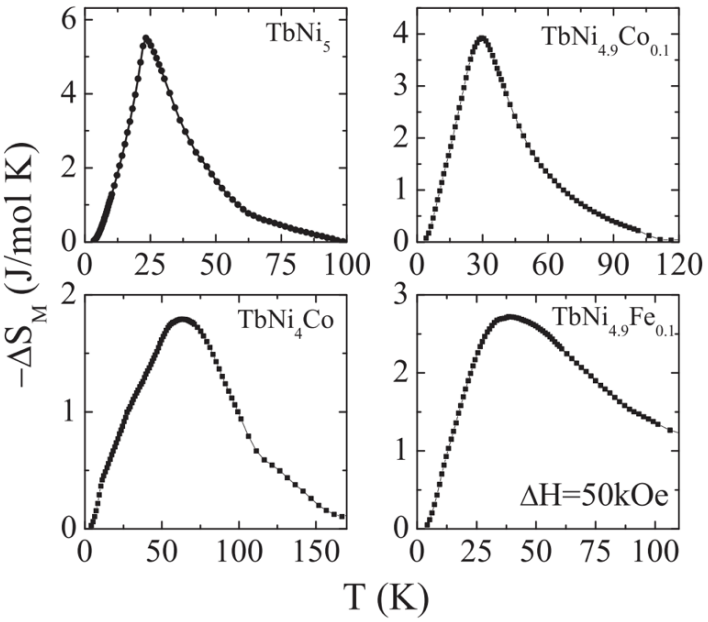

Figure 24. ***Entropy Change of Doped*** $TbNi_5$. *Magnetic entropy change relative to temperature for* $TbNi_{5-x}Co_x$ $(x = 0.1, 1)$ *and* $TbNi_{4.9}Fe_{0.1}$ *using a switching H field of 5 T. Figure adapted from [71].*

T_C more than the increase when doped with cobalt, as displayed in figure 24. Furthermore, increasing the doping concentration also leads to a larger climb of T_C, with the alloy $TbNi_4Co$ showing an almost 40 K rise of T_C compared to undoped $TbNi_5$. From figure 24 it is also apparent that the substitution of Ni with magnetic elements results in the reduction of the magnetic entropy change. Increasing the doping concentration further diminishes the magnetocaloric response. The substitution with

Fe leads to lower ΔS_{mag} values compared to *Co* substitution. The major benefit of the doping is the substantial increase of the FWHM of the ΔS_{mag} peaks, such that the alloys exhibit MCE across the 20-77 K temperature range. Figure 24 also shows that the peak broadening increases with doping concentration (for the case of cobalt). It is argued that this effect is caused by the broadening of the magnetic transition and the transition metal sublattice spin fluctuations [71].

The effect of doping on the ΔT_{ad} of the alloy is shown in figure 25 to follow a similar relationship to that of ΔS_{mag}. The peak adiabatic temperature change decreases with substitution whereas the peak width increases. It is argued that the broad MCE peaks (with respect to temperature) resulting from doping is due to local variations in magnetic anisotropy and exchange interactions in the alloys [71]. This causes a relatively large magnetic entropy in the material under T_C when no external H field is applied.

In spite of the potential magnetocaloric applications of $ReNi_5$ (especially when doped with magnetic elements), the sustainability of the materials is a significant issue for practicality. Although it is claimed that the material group contains low amounts of rare earth elements, the criticality is such that it is unfeasible to produce sufficient volumes of the compounds [63]. Nonetheless, the comprehensive benefits of magnetic element substitution has been demonstrated with $TbNi_5$ and motivates further research into magnetic doping in other magnetocaloric materials.

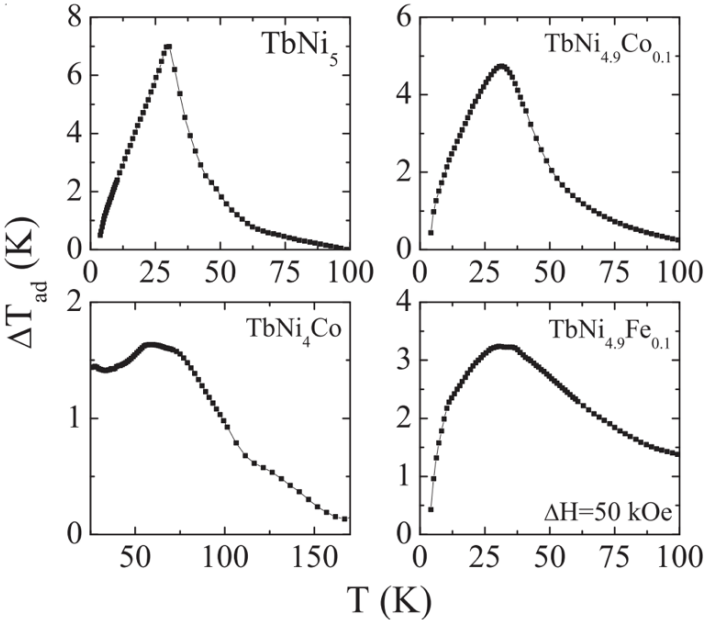

Figure 25. ***Adiabatic Temperature Change of Doped*** $TbNi_5$**.** *T_{ad} change relative to temperature for $TbNi_{5-x}Co_x$ ($x = 0.1, 1$) and $TbNi_{4.9}Fe_{0.1}$ using a switching H field of 5 T. Figure adapted from [71].*

5. Conclusions and Outlook

Of the hundreds of different materials that exhibit the magnetocaloric effect in the appropriate temperature range for hydrogen liquefaction, only a handful can be considered to be sustainable for application [7]. These materials have been analysed for their magnetocaloric properties, with the performance encapsu-

Magnetocaloric Material	T_C (K)	ΔS_{mag} $(JKg^{-1}K^{-1})$	ΔT_{ad} (K)	RCP (JKg^{-1})	Magnetic field strength (T)	Source
Spinel Compounds						
MnV_2O_4	57	14.8	2.9	46.7	2	[54]
$MnV_{1.95}Al_{0.05}O_4$	59.6	5.2	1.5	82.2	2	[56]
$Mn_{0.9}Fe_{0.1}V_2O_4$	59	3.8	-	110	2	[57]
High Entropy Alloy						
$(FeMnNi)_{66.6}(Ge_{0.45}Si_{0.55})_{33.3}$	203	13.1	-	-	2.5	[60]
$FeCoCr_{0.85-1.15}Ni$	40-190	0.33-0.39	-	-	2	[61]
Light Rare Earth Compounds						
$LreAl_2$ $(Lre: Nd, Pr, Ce)$	13.2-78.5	3.67-10.48	~1-2.5	-	2	[63]
$0.292(PrAl_2)+0.708(NdAl_2)$	32.5-77	~1.4	-	-	5	[66]
***ReNi*$_5$ Compounds**						
$GdNi_5$	32	~2.25	~5.5	-	5	[70]
$NdNi_5$	8	~1.58	~4	-	5	[70]
$PrNi_5$	21	~0.091	~0.35	-	5	[70]
$TbNi_{4.9}Fe_{0.1}$	49	~1.22	33	-	5	[71]
Benchmark Rare Earth						
HoB_2	15	24	6	-	2	[45]

Table 1. ***Comparison of Sustainable Magnetocaloric Materials for Hydrogen Liquefaction.*** *A presetation of the parameter values to evaluate the magnetocaloric effect for the materials investigated in this review.*

lated in table 1. The scarcity of prospective materials proves the challenge in developing rare earth free magnetocaloric materials for hydrogen liquefaction, and stresses the need for further material research.

The spinel vanadium oxide and two different high entropy alloys were found as materials completely free of rare earth minerals. However the operating temperature span of these materials were found to be too high for hydrogen liquefaction.

On the other hand, materials were found with the appropriate temperature range, that although contained rare earth elements, have capabilities for sustainability. Although these prospective materials are suitable for hydrogen liquefaction, critical studies into the fabrication processes of these compounds need to be made, in order to establish their potential for application.

The tuning of the transition temperature is possible by substituting elements in magnetocaloric materials. Hereby, if the magnetic exchange interaction is decreased, the ordering temperature also drops. Various different investigations into the affects of doping on the MCE were analysed, studies into magnetic and nonmagnetic dopants in magnetocaloric materials were found to successfully change the magnetocaloric profile. Further experimentation into the capabilities of doping are motivated to investigate how high doping concentrations affect magnetocaloric materials.

The major drawback of doping is the significant reduction in the magnitude of the MCE, as is displayed in table 1. This significantly limits the capabilities of prospective sustainable materials as magnetic refrigerants, thus driving the need to understand the mechanisms behind the MCE in order to facilitate optimization. Materials where the magnetic properties are coupled to the crystallographic degrees of freedom (as is often the case for first-order transitions) were found to exhibit a large magnetocaloric response [72]. The strong spin-lattice coupling gives rise to the simultaneous change in magnetic and lattice entropy upon the switching of a magnetic field. Incorporating this coupling in materials while still mitigating the thermal and magnetic hysteresis, would allow for the optimization of the MCE.

In addition, further analysis into the thermal and magnetic hysteresis is necessary for eventual applications in devices. The mechanisms that are responsible are often unique to these materials, complicating research into efforts to diminish these phenomena. However it has been shown that the doping of nonmagnetic Al in MnV_2O_4 leads to structural changes that reduces the hysteresis significantly [56].

Another aspect that is often overlooked is the dependence of the magnetic field strength on the magnitude of the MCE in materials. Practical and economic challenges in the technology of (permanent) magnets restricts the switching magnetic field strength of conventional devices to 2 T [9][63]. Therefore, prospective magnetocaloric materials need to efficient such that the MCE response is substantial even at low fields. Circumstantially, the relevant cryogenic operating temperatures for hydrogen liquefaction facilitates the use of superconducting magnets as the source of the H field, allowing for field strengths of 5 T to be potentially realised [7][63].

While inspecting the relatively narrow magnetocaloric profiles of compounds with respect to temperature, it is evident that designing a material which exhibits the MCE across the entire 20-77 K temperature range is unfeasible. By changing the stoichiometry, a variety of magnetocaloric materials have the potential to span the relevant temperature range. Although this may seem impractical at first, layered magnetic refrigeration devices have been conceptualized and experimentally investigated [73]. An alternative approach would be the utilization of the Ericsson cycle with composites of magnetocaloric materials [66]. The practicality of such refrigeration devices for hydrogen liquefaction needs to be explored.

In order to realise magnetic cooling for hydrogen liquefaction, an avenue for material research is the concept of multicaloric materials [9]. These materials exhibit entropy changes under the influence of multiple external stimulants, examples include magnetostructural and magnetoelectric materials. Multiferroic materials have been shown to exhibit the MCE at cryogenic temperatures [74]. Furthermore, materials are established that have a magnetocaloric response at cryogenic temperatures and known to exhibit electric polarization, yet their magnetoelectric properties have not yet been probed [75]. This proves that there is potential materials that can be categorized as multicaloric. The challenge is that in order to achieve the cross-response of multicalorics from different fields, the ferroic orders need to be strongly coupled to one another, which requires the understanding of rather complex mechanisms [76].

Furthermore, magnetocaloric materials have been fabricated using novel techniques that may aid in altering their MCE specifications for hydrogen liquefaction [18]. Synthesizing these materials as nanoparticles have been shown to broaden the temperature range across which a substantial entropy change is exhibited [12]. This has been attributed to the reduction of exchange interactions such that the transition temperature is also decreased. These production techniques have a range of consequences, that are often unique to the material onto which they are applied to.

References

[1] P. Nema, S. Nema, and P. Roy, "An overview of global climate changing in current scenario and mitigation action", *Renewable and Sustainable Energy Reviews*, vol. 16, no. 4, pp. 2329–2336, 2012, ISSN: 1364-0321. DOI: https://doi.org/10.1016/j.rser.2012.01.044. [Online]. Available: https://www.sciencedirect.com/science/article/pii/S1364032112000457.

[2] Feb. 2024. [Online]. Available: https://iea.blob.core.windows.net/assets/33e2badc-b839-4c18-84ce-f6387b3c008f/CO2Emissionsin2023.pdf.

[3] M. Aziz, "Liquid hydrogen: A review on liquefaction, storage, transportation, and safety", *Energies*, vol. 14, no. 18, 2021, ISSN: 1996-1073. DOI: 10.3390/en14185917. [Online]. Available: https://www.mdpi.com/1996-1073/14/18/5917.

[4] S. Z. Al Ghafri, S. Munro, U. Cardella, *et al.*, "Hydrogen liquefaction: A review of the fundamental physics, engineering practice and future opportunities", *Energy Environ. Sci.*, vol. 15, pp. 2690–2731, 7 2022. DOI: 10.1039/D2EE00099G. [Online]. Available: http://dx.doi.org/10.1039/D2EE00099G.

[5] L. Yin and Y. Ju, "Review on the design and optimization of hydrogen liquefaction processes", *Frontiers in Energy*, vol. 14, Dec. 2019. DOI: 10.1007/s11708-019-0657-4.

[6] K. Mazloomi and C. Gomes, "Hydrogen as an energy carrier: Prospects and challenges", *Renewable and Sustainable Energy Reviews*, vol. 16, no. 5, pp. 3024–3033, 2012, ISSN: 1364-0321. DOI: https://doi.org/10.1016/j.rser.2012.02.028. [Online]. Available: https://www.sciencedirect.com/science/article/pii/S1364032112001220.

[7] C. Romero-Muñiz, J. Y. Law, J. Revuelta-Losada, L. M. Moreno-Ramírez, and V. Franco, "Magnetocaloric materials for hydrogen liquefaction", *The Innovation Materials*, vol. 1, p. 100 045, 3 2023, ISSN: 2959-8737. DOI: 10.59717/j.xinn-mater.2023.100045.

[8] T. Zhang, J. Uratani, Y. Huang, L. Xu, S. Griffiths, and Y. Ding, "Hydrogen liquefaction and storage: Recent progress and perspectives", *Renewable and Sustainable Energy Reviews*, vol. 176, p. 113 204, 2023, ISSN: 1364-0321. DOI: https://doi.org/10.1016/j.rser.2023.113204. [Online]. Available: https://www.sciencedirect.com/science/article/pii/S1364032123000606.

[9] T. Gottschall, K. P. Skokov, M. Fries, *et al.*, "Making a cool choice: The materials library of magnetic refrigeration", *Advanced Energy Materials*, vol. 9, 34 Sep. 2019, Review Paper provided by Blake. Gottschall is also author of more recent papers: https://doi.org/10.1109/INTERMAGShortPapers58606.2023.10228245 10.1088/2515-7655/accb0b., ISSN: 16146840. DOI: 10.1002/aenm.201901322.

[10] L. Septiany and G. R. Blake, "Magnetocaloric effect and critical behavior in arylamine-based copper chloride layered organic-inorganic perovskite", *Journal of Magnetism and Magnetic Materials*, vol. 542, p. 168 598, 2022, ISSN: 0304-8853. DOI: https://doi.org/10.1016/j.jmmm.2021.168598. [Online]. Available: https://www.sciencedirect.com/science/article/pii/S0304885321008428.

[11] T. Numazawa, K. Kamiya, T. Utaki, and K. Matsumoto, "Magnetic refrigerator for hydrogen liquefaction", *Cryogenics*, vol. 62, pp. 185–192, 2014, ISSN: 0011-2275. DOI: https://doi.org/10.1016/j.cryogenics.2014.03.016. [Online]. Available: https://www.sciencedirect.com/science/article/pii/S0011227514000678.

[12] V. Franco, J. Blázquez, J. Ipus, J. Law, L. Moreno-Ramírez, and A. Conde, "Magnetocaloric effect: From materials research to refrigeration devices", *Progress in Materials Science*, vol. 93, pp. 112–232, 2018, ISSN: 0079-6425. DOI: https://doi.org/10.1016/j.pmatsci.2017.10.005. [Online]. Available: https://www.sciencedirect.com/science/article/pii/S0079642517301299.

[13] S. Blundell, S. Blundell, and K. Blundell, *Concepts in Thermal Physics* (Comprehensive Assessment of Water Management in Agriculture). Oxford University Press, 2006, ISBN: 9780198567691. [Online]. Available: https://books.google.nl/books?id=oaDdswEACAAJ.

[14] J. Y. Law, L. M. Moreno-Ramírez, Á. Díaz-García, and V. Franco, "Current perspective in magnetocaloric materials research", *Journal of Applied Physics*, vol. 133, no. 4, p. 040 903, Jan. 2023, ISSN: 0021-8979. DOI: 10.1063/5.0130035. eprint: https://pubs.aip.org/aip/jap/article-pdf/doi/10.1063/5.0130035/16766788/040903_1_online.pdf. [Online]. Available: https://doi.org/10.1063/5.0130035.

[15] P. Baptista de Castro, K. Terashima, T. Yamamoto, *et al.*, "Machine-learning-guided discovery of the gigantic magnetocaloric effect in hob2 near the hydrogen liquefaction temperature", *NPG Asia Materials*, vol. 12, p. 35, Dec. 2020. DOI: 10.1038/s41427-020-0214-y.

[16] A. Tishin, Y. Spichkin, V. Zverev, and P. Egolf, "A review and new perspectives for the magnetocaloric effect: New materials and local heating and cooling inside the human body", *International Journal of Refrigeration*, vol. 68, pp. 177–186, 2016, ISSN: 0140-7007. DOI: https://doi.org/10.1016/j.ijrefrig.2016.04.020. [Online]. Available: https://www.sciencedirect.com/science/article/pii/S0140700716300615.

[17] G. Xie, L. Wang, B. Li, C. Zhang, and X. Zhang, "Transform commercial magnetic materials into injectable gel for magnetic hyperthermia therapy in vivo", *Colloids and Surfaces B: Biointerfaces*, vol. 224, p. 113 185, 2023, ISSN: 0927-7765. DOI: https://doi.org/10.1016/j.colsurfb.2023.113185. [Online]. Available: https://www.sciencedirect.com/science/article/pii/S0927776523000632.

[18] D. Kim, J. Ahn, B. Sinha, J. Kim, and C. Choi, "Novel route to prepare hon nanoparticles for magnetic refrigerant in cryogenic temperature", *International Journal of Hydrogen Energy*, vol. 40, no. 35, pp. 11 465–11 469, 2015, ISSN: 0360-3199. DOI: https://doi.org/10.1016/j.ijhydene.2015.03.052. [Online]. Available: https://www.sciencedirect.com/science/article/pii/S0360319915006497.

[19] T. Graedel, R. Barr, C. Chandler, *et al.*, "Methodology of metal criticality determination", *Environmental science technology*, vol. 46, pp. 1063–70, Dec. 2011. DOI: 10.1021/es203534z.

[20] W. Leal Filho, R. Kotter, P. G. Özuyar, I. R. Abubakar, J. H. P. P. Eustachio, and N. R. Matandirotya, "Understanding rare earth elements as critical raw materials", *Sustainability*, vol. 15, no. 3, 2023, ISSN: 2071-1050. DOI: 10.3390/su15031919. [Online]. Available: https://www.mdpi.com/2071-1050/15/3/1919.

[21] A. Smith, "Who discovered the magnetocaloric effect?: Warburg, weiss, and the connection between magnetism and heat", English, *European Physical Journal H*, vol. 38, no. 4, pp. 507–517, 2013, ISSN: 2102-6459. DOI: 10.1140/epjh/e2013-40001-9.

[22] E. Warburg, "Magnetische untersuchungen", *Annalen der Physik*, vol. 249, no. 5, pp. 141–164, 1881. DOI: https://doi.org/10.1002/andp.18812490510. eprint: https://onlinelibrary.wiley.com/doi/pdf/10.1002/andp.18812490510. [Online]. Available: https://onlinelibrary.wiley.com/doi/abs/10.1002/andp.18812490510.

[23] P. Weiss and A. Piccard, "Le phénomène magnétocalorique", *J. Phys. Theor. Appl.*, vol. 7, no. 1, pp. 103–109, 1917. DOI: 10.1051/jphystap:019170070010300. [Online]. Available: https://hal.science/jpa-00241982.

[24] P. Debye, "Einige bemerkungen zur magnetisierung bei tiefer temperatur", *Annalen der Physik*, vol. 386, no. 25, pp. 1154–1160, 1926. DOI: https://doi.org/10.1002/andp.19263862517. eprint: https://onlinelibrary.wiley.com/doi/pdf/10.1002/andp.19263862517. [Online]. Available: https://onlinelibrary.wiley.com/doi/abs/10.1002/andp.19263862517.

[25] W. F. Giauque, "A thermodynamic treatment of certain magnetic effects. a proposed method of producing temperatures considerably below 1° absolute", *Journal of the American Chemical Society*, vol. 49, no. 8, pp. 1864–1870, 1927. DOI: 10.1021/ja01407a003. eprint: https://doi.org/10.1021/ja01407a003. [Online]. Available: https://doi.org/10.1021/ja01407a003.

[26] K. Ohira, K. Nakamichi, and H. Furumoto, "Experimental study on magnetic refrigeration for the liquefaction of hydrogen", in *Advances in Cryogenic Engineering*, Q.-S. Shu, Ed. Boston, MA: Springer US, 2000, pp. 1747–1754, ISBN: 978-1-4615-4215-5. DOI: 10.1007/978-1-4615-4215-5_101. [Online]. Available: https://doi.org/10.1007/978-1-4615-4215-5_101.

[27] K. Kamiya, T. Numazawa, H. Takahashi, H. Nozawa, and T. Yanagitani, "Hydrogen liquefaction by magnetic refrigeration", International Cryocooler Conference, 2007. [Online]. Available: https://minds.wisconsin.edu/bitstream/handle/1793/21698/82.pdf?sequence=1.

[28] K. Buschow and F. de Boer, *Physics of Magnetism and Magnetic Materials* (Focus on biotechnology). Springer US, 2007, ISBN: 9780306484087. [Online]. Available: https://books.google.nl/books?id=o_fZBwAAQBAJ.

[29] B. Christopher, "Magnetocaloric effect in thin films and heterostructures", Ph.D. dissertation, 2011. [Online]. Available: https://digitalcommons.usf.edu/etd/3003/.

[30] J. R. Centre, I. for Energy, Transport, *et al.*, *Critical metals in the path towards the decarbonisation of the EU energy sector – Assessing rare metals as supply-chain bottlenecks in low-carbon energy technologies*. Publications Office, 2013. DOI: doi/10.2790/46338.

[31] F. Casanova i Fernàndez, "Magnetocaloric effect in gd5(sixge1-x)4 alloys", Ph.D. dissertation, 2004. [Online]. Available: https://www.tesisenred.net/handle/10803/1789#page=12.

[32] P. J. von Ranke, V. K. Pecharsky, and K. A. Gschneidner, "Influence of the crystalline electrical field on the magnetocaloric effect of $DyAl_2$, $ErAl_2$, and $DyNi_2$", *Phys. Rev. B*, vol. 58, pp. 12 110–12 116, 18 Nov. 1998. DOI: 10.1103/PhysRevB.58.12110. [Online]. Available: https://link.aps.org/doi/10.1103/PhysRevB.58.12110.

[33] K. Bartholomé, *Magnetocaloric systems*, Oct. 2022. [Online]. Available: https://www.ipm.fraunhofer.de/en/bu/energy-converters-thermal/expertise/caloric-systems/magnetocaloric-systems.html.

[34] R. Bozorth, *Ferromagnetism* (Bell Telephone Laboratories series). Van Nostrand, 1951. [Online]. Available: https://books.google.nl/books?id=ny5RAAAAMAAJ.

[35] J. Romero Gómez, R. Ferreiro Garcia, A. De Miguel Catoira, and M. Romero Gómez, "Magnetocaloric effect: A review of the thermodynamic cycles in magnetic refrigeration", *Renewable and Sustainable Energy Reviews*, vol. 17, pp. 74–82, 2013, ISSN: 1364-0321. DOI: https://doi.org/10.1016/j.rser.2012.09.027. [Online]. Available: https://www.sciencedirect.com/science/article/pii/S136403211200528X.

[36] V. K. Pecharsky and K. A. Gschneidner, "Magnetocaloric effect from indirect measurements: Magnetization and heat capacity", *Journal of Applied Physics*, vol. 86, pp. 565–575, 1 1999, ISSN: 00218979. DOI: 10.1063/1.370767.

[37] S. K. Çetin, M. Acet, M. Güneş, A. Ekicibil, and M. Farle, "Magnetocaloric effect in (la1-xsmx)0.67pb0.33mno3 (0 x 0.3) manganites near room temperature", *Journal of Alloys and Compounds*, vol. 650, pp. 285–294, Jul. 2015, ISSN: 09258388. DOI: 10.1016/j.jallcom.2015.07.217.

[38] A. Biswas, A. Thayer, O. Dolotko, and Y. Mudryk, "Borderline first-order phase transition and large cryogenic magnetocaloric effect in prndin", *JOURNAL OF APPLIED PHYSICS*, vol. 134, no. 9, Sep. 2023, ISSN: 0021-8979. DOI: 10.1063/5.0160429.

[39] Y. P. Irkhin, "Electron structure of the 4f shells and magnetism of rare-earth metals", *Soviet Physics Uspekhi*, vol. 31, no. 2, p. 163, Feb. 1988. DOI: 10.1070/PU1988v031n02ABEH005700. [Online]. Available: https://dx.doi.org/10.1070/PU1988v031n02ABEH005700.

[40] J. Jensen and A. Mackintosh, *Rare Earth Magnetism: Structures and Excitations* (International Series of Monographs on Physics). Clarendon Press, 1991, ISBN: 9780198520276. [Online]. Available: https://books.google.nl/books?id=LbTvAAAAMAAJ.

[41] S. Blundell, *Magnetism in Condensed Matter* (Oxford Master Series in Condensed Matter Physics). OUP Oxford, 2001, ISBN: 9780198505914. [Online]. Available: https://books.google.nl/books?id=OGhGmgEACAAJ.

[42] L. Peters, S. Ghosh, B. Sanyal, *et al.*, "Magnetism and exchange interaction of small rare-earth clusters; tb as a representative", *Scientific Reports*, vol. 6, no. 1, Jan. 2016, ISSN: 2045-2322. DOI: 10.1038/srep19676. [Online]. Available: http://dx.doi.org/10.1038/srep19676.

[43] J. S. Amaral and V. S. Amaral, "Simulating the giant magnetocaloric effect-from mean-field theory to microscopic models", *Frontiers in Materials*, vol. 10, 2023, ISSN: 2296-8016. DOI: 10.3389/fmats.2023.1037396. [Online]. Available: https://www.frontiersin.org/articles/10.3389/fmats.2023.1037396.

[44] W. Liu, K. Skokov, T. Gottschall, A. Aubert, F. Scheibel, and O. Gutfleisch, "Giant magnetocaloric effects of 2nd order phase transition utilized for liquefaction of hydrogen near 20 k", in *2023 IEEE International Magnetic Conference - Short Papers (INTERMAG Short Papers)*, 2023, pp. 1–2. DOI: 10.1109/INTERMAGShortPapers58606.2023.10228245.

[45] P. Baptista de Castro, K. Terashima, T. Yamamoto, *et al.*, "Machine-learning-guided discovery of the gigantic magnetocaloric effect in hob2 near the hydrogen liquefaction temperature", *NPG Asia Materials*, vol. 12, p. 35, Dec. 2020. DOI: 10.1038/s41427-020-0214-y.

[46] B. Biswas, D. Biswas, M. Debnath, E. Bose, and S. Pal, "Giant magnetocaloric effect and second order phase transition in prmno3", *Journal of Magnetism and Magnetic Materials*, vol. 588, Dec. 2023, ISSN: 03048853. DOI: 10.1016/j.jmmm.2023.171445.

[47] A. Kartashev, I. Flerov, N. Volkov, and K. Sablina, "Adiabatic calorimetric study of the intense magnetocaloric effect and the heat capacity of (la0.4eu0.6)0.7pb0.3mno3", *Physics of the Solid State*, vol. 50, pp. 2115–2120, Jan. 2008. DOI: 10.1134/S1063783408110188.

[48] A. Arrott, "Criterion for ferromagnetism from observations of magnetic isotherms", *Phys. Rev.*, vol. 108, pp. 1394–1396, 6 Dec. 1957. DOI: 10.1103/PhysRev.108.1394. [Online]. Available: https://link.aps.org/doi/10.1103/PhysRev.108.1394.

[49] B. Banerjee, "On a generalised approach to first and second order magnetic transitions", *Physics Letters*, vol. 12, no. 1, pp. 16–17, 1964, ISSN: 0031-9163. DOI: https://doi.org/10.1016/0031-9163(64)91158-8. [Online]. Available: https://www.sciencedirect.com/science/article/pii/0031916364911588.

[50] Y. Zhang, W. Hao, C. Hu, X. Wang, X. Zhang, and L. Li, "Rare-earth-free mn30fe20xcuxal50 magnetocaloric materials with stable cubic cscl-type structure for room-temperature refrigeration", *Advanced Functional Materials*, vol. 33, no. 52, p. 2 310 047, 2023. DOI: https://doi.org/10.1002/adfm.202310047. eprint: https://onlinelibrary.wiley.com/doi/pdf/10.1002/adfm.202310047. [Online]. Available: https://onlinelibrary.wiley.com/doi/abs/10.1002/adfm.202310047.

[51] I. Park and S. Jeong, "Experimental investigation of 20 k two-stage layered active magnetic regenerative refrigerator", *IOP Conference Series: Materials Science and Engineering*, vol. 101, p. 012 106, Dec. 2015. DOI: 10.1088/1757-899X/101/1/012106.

[52] G. Pilania, V. Kocevski, J. Valdez, C. Kreller, and B. Uberuaga, "Prediction of structure and cation ordering in an ordered normal-inverse double spinel", *Communications Materials*, vol. 1, Nov. 2020. DOI: 10.1038/s43246-020-00082-2.

[53] L. Zhang, H. Han, Z. Qu, *et al.*, "Critical behavior of spinel MnV2O4 investigated by dc-magnetization", *Journal of Applied Physics*, vol. 115, no. 23, p. 233 910, Jun. 2014, ISSN: 0021-8979. DOI: 10.1063/1.4884339. eprint: https://pubs.aip.org/aip/jap/article-pdf/doi/10.1063/1.4884339/15140453/233910_1_online.pdf. [Online]. Available: https://doi.org/10.1063/1.4884339.

[54] X. Luo, Y. P. Sun, L. Hu, *et al.*, "Observation of the large magnetocaloric effect in an orbital–spin-coupled system mnv2o4", *Journal of Physics: Condensed Matter*, vol. 21, no. 43, p. 436 010, Oct. 2009. DOI: 10.1088/0953-8984/21/43/436010. [Online]. Available: https://dx.doi.org/10.1088/0953-8984/21/43/436010.

[55] Y. Fu, X. Luo, Z. Huang, *et al.*, "Critical behavior of spinel vanadate mnv1.95al0.05o4", *Journal of Magnetism and Magnetic Materials*, vol. 326, pp. 205–209, 2013, ISSN: 0304-8853. DOI: https://doi.org/10.1016/j.jmmm.2012.08.013. [Online]. Available: https://www.sciencedirect.com/science/article/pii/S0304885312006749.

[56] X. Luo, W. Lu, Z. Huang, *et al.*, "Large reversible magnetocaloric effect in spinel mnv2o4 with minimal al substitution", *Journal of Magnetism and Magnetic Materials*, vol. 324, no. 5, pp. 766–769, 2012, ISSN: 0304-8853. DOI: https://doi.org/10.1016/j.jmmm.2011.09.013. [Online]. Available: https://www.sciencedirect.com/science/article/pii/S0304885311006718.

[57] Z. H. Huang, X. Luo, L. Hu, *et al.*, "Observation of the large magnetocaloric effect and suppression of orbital entropy change in Fe-doped MnV2O4", *Journal of Applied Physics*, vol. 115, no. 3, p. 034 903, Jan. 2014, ISSN: 0021-8979. DOI: 10.1063/1.4861630. eprint: https://pubs.aip.org/aip/jap/article-pdf/doi/10.1063/1.4861630/15130817/034903_1_online.pdf. [Online]. Available: https://doi.org/10.1063/1.4861630.

[58] J. Y. Law, L. M. Moreno-Ramírez, Á. Díaz-García, *et al.*, "Mnfenigesi high-entropy alloy with large magnetocaloric effect", *Journal of Alloys and Compounds*, vol. 855, p. 157 424, 2021, ISSN: 0925-8388. DOI: https://doi.org/10.1016/j.jallcom.2020.157424. [Online]. Available: https://www.sciencedirect.com/science/article/pii/S0925838820337889.

[59] J. Y. Law and V. Franco, "Review on magnetocaloric high-entropy alloys: Design and analysis methods", *Journal of Materials Research*, vol. 38, pp. 37–51, Sep. 2022. DOI: 10.1557/s43578-022-00712-0.

[60] J. Y. Law, Á. Díaz-García, L. M. Moreno-Ramírez, and V. Franco, "Increased magnetocaloric response of femnnigesi high-entropy alloys", *Acta Materialia*, vol. 212, p. 116 931, 2021, ISSN: 1359-6454. DOI: https://doi.org/10.1016/j.actamat.2021.116931. [Online]. Available: https://www.sciencedirect.com/science/article/pii/S1359645421003116.

[61] M. S. Lucas, D. Belyea, C. Bauer, *et al.*, "Thermomagnetic analysis of FeCoCrxNi alloys: Magnetic entropy of high-entropy alloys", *Journal of Applied Physics*, vol. 113, no. 17, 17A923, Mar. 2013, ISSN: 0021-8979. DOI: 10.1063/1.4798340. eprint: https://pubs.aip.org/aip/jap/article-pdf/doi/10.1063/1.4798340/13976295/17a923_1_online.pdf. [Online]. Available: https://doi.org/10.1063/1.4798340.

[62] L. Omodara, S. Pitkäaho, E.-M. Turpeinen, P. Saavalainen, K. Oravisjärvi, and R. L. Keiski, "Recycling and substitution of light rare earth elements, cerium, lanthanum, neodymium, and praseodymium from end-of-life applications - a review", *Journal of Cleaner Production*, vol. 236, p. 117 573, 2019, ISSN: 0959-6526. DOI: https://doi.org/10.1016/j.jclepro.2019.07.048. [Online]. Available: https://www.sciencedirect.com/science/article/pii/S095965261932387X.

[63] W. Liu, T. Gottschall, F. Scheibel, *et al.*, "Designing magnetocaloric materials for hydrogen liquefaction with light rare-earth laves phases", *Journal of Physics: Energy*, vol. 5, no. 3, p. 034 001, May 2023. DOI: 10.1088/2515-7655/accb0b. [Online]. Available: https://dx.doi.org/10.1088/2515-7655/accb0b.

[64] M. de Souza, "Investigation on the magnetocaloric effect in rni2 (r: Dy, tb) melt-spun ribbon", *Journal of Magnetism and Magnetic Materials*, vol. 412, pp. 11–14, 2016, ISSN: 0304-8853. DOI: https://doi.org/10.1016/j.jmmm.2016.03.078. [Online]. Available: https://www.sciencedirect.com/science/article/pii/S0304885316302852.

[65] P. J. von Ranke and W. S. Torres, "Theoretical investigation of crystalline electric field influence on the magnetocaloric effect in the cubic praseodymium system $PrNi_2$", *Phys. Rev. B*, vol. 105, p. 085 153, 8 Feb. 2022. DOI: 10.1103/PhysRevB.105.085153. [Online]. Available: https://link.aps.org/doi/10.1103/PhysRevB.105.085153.

[66] A. M. G. Carvalho, J. C. P. Campoy, A. A. Coelho, E. J. R. Plaza, S. Gama, and P. J. von Ranke, "Experimental and theoretical analyses of PrAl2 and NdAl2 composite for use as an active magnetic regenerator", *Journal of Applied Physics*, vol. 97, no. 8, p. 083 905, Apr. 2005, ISSN: 0021-8979. DOI: 10.1063/1.1876575. eprint: https://pubs.aip.org/aip/jap/article-pdf/doi/10.1063/1.1876575/14949163/083905_1_online.pdf. [Online]. Available: https://doi.org/10.1063/1.1876575.

[67] P. J. Ibarra-Gaytán, J. L. Sánchez Llamazares, P. Álvarez-Alonso, C. F. Sánchez-Valdés, P. Gorria, and J. A. Blanco, "Magnetic entropy table-like shape in RNi2 composites for cryogenic refrigeration", *Journal of Applied Physics*, vol. 117, no. 17, p. 17C116, Mar. 2015, ISSN: 0021-8979. DOI: 10.1063/1.4915480. eprint: https://pubs.aip.org/aip/jap/article-pdf/doi/10.1063/1.4915480/15159512/17c116_1_online.pdf. [Online]. Available: https://doi.org/10.1063/1.4915480.

[68] J. Liu and E. Huston, "Rni5 hydrogen storage compounds (r rare earth)", *Journal of the Less Common Metals*, vol. 90, no. 1, pp. 11–20, 1983, ISSN: 0022-5088. DOI: https://doi.org/10.1016/0022-5088(83)90111-X. [Online]. Available: https://www.sciencedirect.com/science/article/pii/002250888390111X.

[69] K. Buschow and A. Van der Goot, "Composition and crystal structure of hexagonal cu-rich rare earth–copper compounds", *Acta Crystallographica Section B: Structural Crystallography and Crystal Chemistry*, vol. 27, no. 6, pp. 1085–1088, 1971. DOI: https://doi.org/10.1107/S0567740871003558.

[70] P. Ranke, M. Mota, D. Grangeia, *et al.*, "Magnetocaloric effect in the r ni5 (r=pr , nd, gd, tb, dy, ho, er) series", *Physical Review B*, vol. 70, p. 134 428, Sep. 2004. DOI: 10.1103/PhysRevB.70.134428.

[71] A. Haldar, I. Dhiman, A. Das, K. Suresh, and A. Nigam, "Magnetic, magnetocaloric and neutron diffraction studies on tbni5xmx (m=co and fe) compounds", *Journal of Alloys and Compounds*, vol. 509, no. 9, pp. 3760–3765, 2011, ISSN: 0925-8388. DOI: https://doi.org/10.1016/j.jallcom.2011.01.012. [Online]. Available: https://www.sciencedirect.com/science/article/pii/S0925838811000338.

[72] L. Patra and B. Liao, "Indirect exchange interaction leads to large lattice contribution to magnetocaloric entropy change", *Physical Review Letters*, vol. 131, no. 6, Aug. 2023, ISSN: 1079-7114. DOI: 10.1103/physrevlett.131.066703. [Online]. Available: http://dx.doi.org/10.1103/PhysRevLett.131.066703.

[73] D. Pineda Quijano, C. Infante Ferreira, and E. Brück, "Layering strategies for active magnetocaloric regenerators using mnfepsi for heat pump applications", *Applied Thermal Engineering*, vol. 232, p. 120 962, 2023, ISSN: 1359-4311. DOI: https://doi.org/10.1016/j.applthermaleng.2023.120962. [Online]. Available: https://www.sciencedirect.com/science/article/pii/S1359431123009912.

[74] K. Dey, A. Indra, S. Majumdar, and S. Giri, "Critical behavior and reversible magnetocaloric effect in multiferroic mncr2o4", *Journal of Magnetism and Magnetic Materials*, vol. 435, pp. 15–20, 2017, ISSN: 0304-8853. DOI: https://doi.org/10.1016/j.jmmm.2017.03.068. [Online]. Available: https://www.sciencedirect.com/science/article/pii/S0304885316324878.

[75] S. Mansouri, M. Balli, S. Jandl, *et al.*, "On the magnetocaloric effect and the spin-phonon coupling in the multiferroic gdmn2o5", *Journal of Alloys and Compounds*, vol. 961, p. 170 955, 2023, ISSN: 0925-8388. DOI: https://doi.org/10.1016/j.jallcom.2023.170955. [Online]. Available: https://www.sciencedirect.com/science/article/pii/S0925838823022582.

[76] A. Planes, T. Castn, and A. Saxena, "Thermodynamics of multicaloric effects in multiferroic materials: Application to metamagnetic shape-memory alloys and ferrotoroidics", *Philosophical Transactions of the Royal Society A: Mathematical, Physical and Engineering Sciences*, vol. 374, p. 20 150 304, Aug. 2016. DOI: 10.1098/rsta.2015.0304.